



**ELECTRON MULTIFACTOR: THEORY REVIEW, COMPARISON  
AND MODELING OF MITIGATION TECHNIQUES IN ICEPIC**

THESIS

Neil Rogers, Captain, USAF  
AFIT/GE/ENP/09-M02

**DEPARTMENT OF THE AIR FORCE  
AIR UNIVERSITY**

**AIR FORCE INSTITUTE OF TECHNOLOGY**

**Wright-Patterson Air Force Base, Ohio**

APPROVED FOR PUBLIC RELEASE; DISTRIBUTION UNLIMITED.

The views expressed in this thesis are those of the author and do not reflect the official policy or position of the United States Air Force, Department of Defense, or the United States Government.

AFIT/GE/ENP/09-M02

**ELECTRON MULTIFACTOR: THEORY REVIEW, COMPARISON  
AND MODELING OF MITIGATION TECHNIQUES IN ICEPIC**

THESIS

Presented to the Faculty  
Department of Engineering Physics  
Graduate School of Engineering and Management  
Air Force Institute of Technology  
Air University  
Air Education and Training Command  
in Partial Fulfillment of the Requirements for the  
Degree of Master of Science in Electrical Engineering

Neil Rogers, BSEE  
Captain, USAF

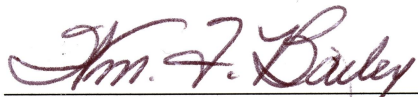
March 2009

APPROVED FOR PUBLIC RELEASE; DISTRIBUTION UNLIMITED.

**ELECTRON MULTIPACTOR: THEORY REVIEW, COMPARISON  
AND MODELING OF MITIGATION TECHNIQUES IN ICEPIC**

Neil Rogers, BSEE  
Captain, USAF

Approved:



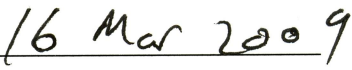
William F. Bailey (Chairman)



Date



Stephen C. Cain (Member)



Date



Michael J. Havrilla (Member)



Date

## **Abstract**

Single surface multipactor is a phenomenon which imposes a limit on the total power that may be transmitted by a High Powered Microwave (HPM) System. Electron multipactor results in an avalanche of high energy electrons within the waveguide. In a relatively short time, the electrons deposit power on the surface of the dielectric window which separates the waveguide from the antenna and, eventually, the window can be damaged and the system will fail. Mitigation approaches for single surface multipactor at dielectric windows are investigated using Particle-In-Cell (PIC) simulations. Initially baseline susceptibility diagrams are constructed analytically and compared with self-consistent, dynamic system trajectories. The power deposited on the surface of a dielectric window in an HPM system is considered using three different methods and the results of PIC simulations. Geometric mitigation is then considered by varying the window orientation with respect to the HPM electric field. Small angular deviations, less than 20 degrees, from the nominal case of normal incidence show dramatic changes in the susceptibility diagram. A materials approach to mitigation is then considered. Titanium Nitride, TiN, coatings applied to the dielectric surface can substantially reduce the secondary emission yield. Representative modifications of the secondary emission yield are simulated and the resulting susceptibility diagrams are discussed.

## Acknowledgements

First and foremost, I owe a large debt of gratitude to God, for without His constant provision, I would be lost. I would also like to thank Dr. Bailey, my advisor, whose door was always open for lengthy discussions. He was willing to teach an Electrical Engineer how to think like a Physicist (for the most part), and impart wisdom from his seemingly endless stores of knowledge. Indeed, I have heard horror stories about thesis advisors, but my experience was quite the opposite - finding mine to be accessible, flexible, congenial and, most of all, patient. The support of the HPM division (AFRL/RDHE) has been crucial in understanding the simulation methods, interpreting our results, and providing funding for this research. I look forward to joining their ranks soon.

I am very thankful for my family, both near and far, who supported us through the birth of our son and this "interesting" endeavor called writing a thesis. My lovely wife was consistently forebearing and supportive through a few long weeks of unprecedented stress in our house. She is a wonderful wife and a fine mother. Finally, I would be remiss in forgetting Brian Witthoeft, who was always willing to check me on anything; as well as Brook, Mitch, Kaitie and Spencer, with whom I have spent many hours laboring away in the Aero lab and who were willing sounding boards for problems and who were, perhaps more importantly, a continual source of laughter and random conversation. This thesis is dedicated to the giants on whose shoulders we stand and to those who follow in my small footsteps - may your success be greater than mine.

Neil Rogers

# Table of Contents

	Page
I. Introduction . . . . .	1
1.1 Problem Description . . . . .	1
1.2 Background . . . . .	1
1.3 Mitigation Concepts . . . . .	3
1.4 Research Goals . . . . .	3
II. Multipactor Theory . . . . .	5
2.1 RF Cavity Multipactor . . . . .	5
2.2 Single Surface Multipactor . . . . .	6
2.2.1 Conventions, Notations and Definitions . . . . .	7
2.2.2 Secondary Emission . . . . .	9
2.2.3 Kinematic Theory . . . . .	10
2.2.4 Interpretation and Characterization of Multipactor . . . . .	17
2.2.5 Mitigation Methods . . . . .	24
III. Computational Models and Comparison with Theory . . . . .	30
3.1 ICEPIC Input Parameters . . . . .	30
3.1.1 Defaults and Variables . . . . .	31
3.1.2 [Time] Section . . . . .	31
3.1.3 System Geometry . . . . .	32
3.1.4 Plane Wave Emission . . . . .	34
3.1.5 Particle Emission . . . . .	35
3.1.6 Dump Parameters . . . . .	38
3.1.7 The [Expert] Section . . . . .	39
3.1.8 ICEPIC Code Updates . . . . .	40
3.2 Comparison of Results . . . . .	41
3.2.1 Non-Space Charge (NSC) Case . . . . .	41
3.2.2 Space Charge Case . . . . .	45
3.2.3 Power Deposition on the Dielectric Surface . . . . .	49
3.3 Mitigation Methods . . . . .	54
3.3.1 Thin Coatings of Low-SEY Materials . . . . .	54
3.3.2 Geometrical Modification of the Waveguide/Window Interface . . . . .	54
IV. Analysis of Results . . . . .	60
4.1 Multipactor Power . . . . .	60
4.1.1 Power Deposition . . . . .	61
4.1.2 Reflected Power . . . . .	61

	Page
4.1.3 Multipactor Power Limit versus Air Breakdown Limit . . . . .	62
4.2 Mitigation Techniques . . . . .	63
4.2.1 Geometric Modification of the Waveguide/Window Interface . . . . .	63
4.2.2 Thin Coatings of Low-SEY Materials . . . . .	64
V. Conclusions and Future Work . . . . .	68
5.1 Conclusions . . . . .	68
5.2 Future Work . . . . .	71
A. Sample ICEPIC Input File for Non-Space Charge Case . . . . .	73
B. Sample ICEPIC Input File for Space Charge Case . . . . .	77
C. Code for Calculation of Theoretical Susceptibility Curves for the Oblique Case in MATLAB <sup>®</sup> . . . . .	84
D. Input File for the Oblique Case in ICEPIC . . . . .	92
E. Mathematica <sup>®</sup> Notebook for the Approximation of the Theoretical Power Deposited on the Surface of a Dielectric . . . . .	97

## List of Figures

Figure	Page
1. Kishkek and Lau’s equivalent RF circuit [10] . . . . .	6
2. The general geometry for single surface multipactor . . . . .	8
3. The mean impact energy of collected particles . . . . .	11
4. Comparison of three forms of the SEE equations . . . . .	12
5. Figure 2 is shown again for convenience . . . . .	13
6. Kishkek’s universal susceptibility curves [12] . . . . .	18
7. Kim and Verboncoeur’s [9] periodic susceptibility curves . . . . .	21
8. The general mathematical flow of PIC codes . . . . .	22
9. A comparison of secondary emission yield curves . . . . .	26
10. The oblique geometry for single surface multipactor . . . . .	27
11. Secondary emission curve as given by Valfells, et al. [15] . . . . .	29
12. The geometry used for ICEPIC simulations . . . . .	34
13. Comparison with Fichtl’s multipactor boundary curves . . . . .	43
14. Particle growth near the lower multipactor boundary curve . . . . .	44
15. Evolution of fields and particles in a multipactoring system . . . . .	47
16. ”Bowtie” plots from Kim and Verboncoeur [9] . . . . .	48
17. Fraction of input power deposited on the surface . . . . .	50
18. Comparison of the theoretical and ICEPIC fields . . . . .	59
19. Susceptibility curves generated from MATLAB®simulations . . . . .	65
20. Susceptibility curves generated from ICEPIC simulations . . . . .	66
21. Comparison of power deposition for thinly coated dielectric . . . . .	67

## List of Tables

Table		Page
1.	Parameters used for ICEPIC simulations . . . . .	46
2.	Comparison of power deposition metrics . . . . .	54
3.	Parameters used to simulate a thinly coated dielectric surface. . . . .	55

## List of Symbols

Table	Page
$\delta$	Secondary emission yield, also referred to as $\delta(E_i, \zeta)$ . . . . . 8
$\delta_{max0}$	Characteristic secondary emission coefficient . . . . . 3
$E_{DC}$	The field that restores electrons to the dielectric surface . . . . . 2
$E_{RF}$	RF electric field of the HPM system . . . . . 3
$\mathcal{E}_i$	Impact energy of an impinging electron . . . . . 8
$\mathcal{E}_{max}(\zeta)$	Impact energy of an impinging electron . . . . . 8
$\mathcal{E}_{max0}$	Maximum impact energy that produces $\delta_{max0}$ . . . . . 8
$\mathcal{E}_{0m}$	Peak emission energy of secondaries . . . . . 18
$\zeta$	Angle of impact for an impinging electron . . . . . 8
$k_s$	Surface smoothness parameter . . . . . 8
$\psi$	The angle between the dielectric surface and $E_{RF}$ . . . . . 25
$\omega_p$	Plasma frequency . . . . . 8
$\omega$	RF angular frequency of the system . . . . . 8

## List of Abbreviations

Abbreviation		Page
EM	Electro-Magnetic . . . . .	46
RF	Radio Frequency . . . . .	1
SC	Space Charge . . . . .	7
FFT	Fast Fourier Transform . . . . .	22
HPM	High Powered Microwave . . . . .	1
NSC	Non-Space Charge . . . . .	7
PIC	Particle-in-Cell . . . . .	20
PML	Perfectly Matched Layer . . . . .	31
SEE	Secondary Electron Emission . . . . .	67
SEY	Secondary Electron Yield . . . . .	3
Ti:N	Titanium Nitride . . . . .	24
ICEPIC	Improved Concurrent Electromagnetic Particle in-Cell . . . . .	22

# ELECTRON MULTIPACTOR: THEORY REVIEW, COMPARISON AND MODELING OF MITIGATION TECHNIQUES IN ICEPIC

## I. Introduction

### 1.1 Problem Description

Recent technological advances in the study, design and implementation of High Powered Microwave (HPM) Devices have led to increased power levels throughout the entire system. Higher power levels present many problems within the waveguide that transfers the energy between the source and the antenna, most notably breakdown and electron multipactor. In order to prevent breakdown, the waveguide must be kept at very low, near-vacuum pressures. A dielectric window situated at the end of the waveguide maintains the low pressure inside the waveguide, while allowing the Radio Frequency (RF) energy to pass through to the antenna. Single surface multipactor can occur at the surface of this window; which, when combined with thermal heating due to the high power throughput, can lead to cracks in the window and, soon thereafter, catastrophic system failure. Therefore, it is desirable and even necessary, for future systems, to mitigate this phenomenon.

### 1.2 Background

Electron multipactor is a phenomenon first observed in 1934 by Otto Farnsworth [7]. Farnsworth was able to harness the effect to create an "AC electron multiplier," thereby terming the phenomenon "multipactor". The following brief description of electron multipactor will be followed by a more detailed discussion in Chapter II.

Multipactor occurs in two distinct cases: in a waveguide or RF cavity and at a single dielectric surface. In both cases, "seed" electrons are provided by stray electrons emitted by random emission processes (cosmic rays, material emission, etc). In the first case, microwave energy propagates through a (semi-infinite) waveguide cavity, an AC electric field is created between the two sides of the cavity and electrons from one side are accelerated towards the other side. When these energetic electrons strike the surface, more than one electron may be emitted according to Vaughn's formula for secondary emission [17]. This leads to a loading and detuning of the cavity. In the second case, at the surface of a single dielectric, electrons leave the surface of the dielectric, leaving behind an overall positive surface charge. These electrons then gain energy from the microwave field, but are returned to the surface by the restoring field generated by the separated charge in the system (referred to as  $E_{DC}$ ). As in the previous case, upon striking the dielectric surface, more than one electron may be emitted. Overall, as more and more electrons are emitted and strike the surface, they will deposit a certain amount of power on the surface, which can lead to: destruction of the dielectric material and, in the case of High Powered Microwave (HPM) systems, loss of necessary vacuum conditions, perpetuation of further loss mechanisms and eventual failure of the system. According to Barker [3], multipactor is not the sole cause of window failure, rather, it is an enabling process in a series of destructive phenomena that occur under some circumstances in a single-surface geometry.

While general theory attracted a small amount of attention, not until the advent and widespread use of modern microwave devices (especially those at higher powers) was a coherent theory formulated by Vaughn. The culmination of his work [17] is the foundation of multipactor theory and is commonly referenced to describe secondary emission from any given material using a small number of parameters. In the past decade, a small group of researchers (Ang, Lau, Verboncoeur, Kishek, Sanzatov,

Valfells, etc.) have continued to investigate and develop theoretical representations of multipactor. Their work is summarized in Chapter II.

### 1.3 Mitigation Concepts

Mitigation concepts have been investigated in the past, but conclusive data is still lacking in the effectiveness of such strategies. Two strategies are considered in this paper:

- Thin Film Coatings - a thin coating of a material with a low Secondary Electron Yield (SEY), ideally at or near one, is deposited on the surface of the dielectric, with the goal of reducing the amount of electrons produced by multipactor in the system.
- Geometrical Modification of the Waveguide/Window Interface - an angle of obliqueness is introduced between the orientation of the RF field ( $E_{RF}$ ) and the dielectric surface, resulting in a narrowing of the susceptibility of the system to multipactor.

### 1.4 Research Goals

The goal of this thesis is twofold: to investigate previous research efforts, validating both analytical and computational results of those efforts and to seek out methods to prevent electron multipactor or mitigate the effects thereof, in the context of HPM systems. The two primary methods considered for mitigation are: thin coatings of special materials and geometric modifications to the window. Thin coatings of materials with lower secondary emission coefficients,  $\delta_{max0}$ , reduce the overall quantity of secondary electrons. Under some circumstances, this method may prevent the avalanche of secondaries and the deposition of power that results in damage to the

dielectric window. The properties of these materials will be further discussed in Chapter II. The geometric modification method relies on the interaction of the electric fields near the surface of the dielectric surface to alter the susceptibility of a system to multipactor, a result that will also be discussed in detail in Chapter II.

## II. Multipactor Theory

In order to further understand multipactor and to analyze possible mitigation strategies, the analytical theory must be well understood. Current theory on multipactor is well described and documented by a small group of researchers, including, but not limited to: Verboncoeur, Kishkek, Lau, Ang, Fichtl and Kim. A summary of their work and conclusions is presented in this chapter.

### 2.1 RF Cavity Multipactor

While a lengthy discussion of multipactor in a cavity would be productive and informative, the primary focus of this research is on single surface multipactor. However, for completeness, a short discussion of the theory associated with cavity multipactor follows. The effect of multipactor in a cavity system is well-described by Kishkek and Lau [10]. They compare cavity multipactor to an equivalent RF circuit, in which cavity loading and detuning are the primary loss mechanisms. The generic circuit they assume is given in Figure 1, where a single sheet of electrons of density  $\sigma$  traverses the cavity of width  $D$  as time progresses, leading to a (normalized) multipactor current of:

$$I_m(t) = -\sigma(t) \frac{dx(t)}{dt}$$

This current is assumed to be the current which loads the cavity and, therefore, diminishing the RF field as it propagates through the system. This acts as a loss mechanism, reducing the total power output of the HPM system.

The secondary emission of the two surfaces is exactly the same as that for the dielectric surface (given in further detail in Section 2.2). It is determined by Kishkek and Lau [10] that the RF beam loading effects are much more important than the

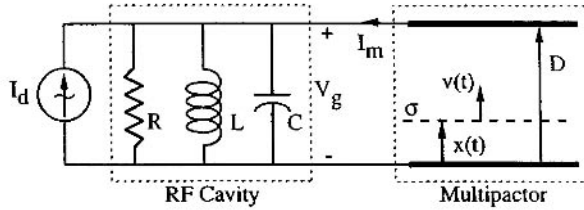


Figure 1. Kishek and Lau's equivalent RF circuit [10]

space charge effects for a high quality factor,  $Q = \frac{1}{R} \sqrt{\frac{L}{C}} > 10$ , and for a small spatial extent,  $x$ , the power delivered to the surfaces by multipactor can be very high. This is a simplistic model, designed only to show that multipactor can indeed deliver power to the walls of the cavity and reduce the output power of the system.

## 2.2 Single Surface Multipactor

Single surface multipactor, such as that occurring at the surface of the dielectric window in an HPM device, is a mechanism resulting in power deposition on the surface of the dielectric, physical damage to the dielectric window and catastrophic failure of the HPM system. The physical consequence of this effect is a limit in the amount of power that may be transported through the waveguide and to the target. It is also worth noting that electron multipactor acts as a beam-loading mechanism, decreasing the total power output of the system.

The geometry for single surface multipactor is given by Figure 2. Since the goal of this research is to reduce the amount of power deposited on the dielectric surface, it is worth noting that early work by Kishek, et al. [10] estimated the power deposited on the dielectric window to be on the order of 1% of the total RF energy. This estimate will be compared with the later analytical developments of multipactor theory. Kishek, et al. were the first to generate susceptibility curves for a wide range of materials. Early developments of multipactor theory relied on a simple, yet

unrealistic assumption that neglected space charge effects. For the purposes of this research, Space Charge (SC) effects refer to the electromagnetic contributions of electrons to the system. Therefore, when space charge is ignored (called the Non-Space Charge (NSC) case), the current density,  $J$  in Ampere's Law, is hard-wired to zero. Physically, this enforces a stationary solution of the charge conservation equation and neglects the influence of the changing electron density. Therefore, the restoring field,  $E_{DC}$ , is not allowed to evolve "naturally", according to the number of electrons in the system, but is assumed to be a constant value. For a complete development of early theory, please see Barker [3] or Fichtl [7]. In order to gain a more fundamental understanding of the complexity of the multipactor problem, this development will start with a description of secondary emission, then move to an analysis of the equations of motion for multipactoring electrons and conclude with an estimation of the power deposited on the surface of the dielectric. This development includes space charge effects.

### 2.2.1 Conventions, Notations and Definitions.

Since the notational conventions vary throughout the literature, the following standards are implemented in describing this work:

- A block  $E$  represents an electric field
- A script  $\mathcal{E}$  represents an energy, such as the impact energy of electrons,  $\mathcal{E}_i$
- A word (or words) set in typewriter font, such as ENERGY, represents an input parameter or section of input parameters, usually to simulation.
- Standard physical quantities, such as mass, acceleration and velocity, are denoted by their usual forms,  $m$ ,  $a$  and  $v$ .

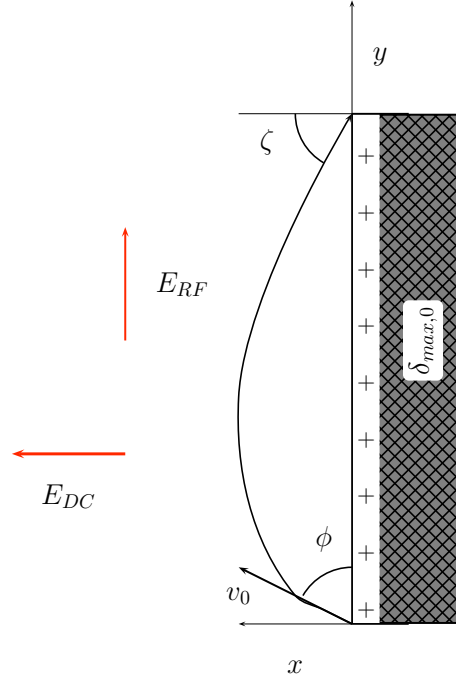


**Figure 2. The general geometry for single surface multipactor**

- Subscripts are used to distinguish similar quantities in a system, or to provide further information about a specific quantity. In this case,  $a_y$  would be a  $y$ -directed acceleration and  $\mathcal{E}_i$  would be the impact energy of an electron.

In order to use clear and consistent notation throughout this paper, definitions for the terms in many of the equations are as follows (exceptions are noted and defined as they are encountered):

$\delta(\mathcal{E}_i, \zeta)$  = the ratio of emitted secondaries to incident electrons as a function of the impact energy and angle

$\delta$  = shorthand for  $\delta(\mathcal{E}_i, \zeta)$

$\delta_{max0}$  = the characteristic secondary emission term

$\mathcal{E}_{max}(\zeta)$  = the impact energy as a function of impact angle

$\mathcal{E}_{max0}$	= the maximum impact energy that produces $\delta_{max0}$
$\zeta$	= the angle of impact, measured from the normal
$\mathcal{E}_i$	= the impact energy of impinging electrons
$k_s$	= a surface smoothness parameter, usually equal to 1
$\omega_p$	= plasma frequency
$\omega$	= RF angular frequency of the system

### 2.2.2 Secondary Emission.

The most commonly accepted form for secondary emission at the dielectric surface is given by Vaughn's model [17]:

$$\delta(\mathcal{E}_i, \zeta) = \delta_{max}(\zeta) \cdot (we^{(1-w)})^{k(w)} \quad (1)$$

$$k = \begin{cases} 0.56 & \text{for } w \leq 1 \\ 0.25 & \text{for } 1 < w \leq 3.6 \end{cases} \quad (2)$$

$$\delta(\mathcal{E}_i, \zeta) = \delta_{max}(\zeta) \cdot (1.125w^{-0.35}) \text{ for } w > 3.6 \quad (3)$$

$$\delta_{max}(\zeta) = \delta_{max0} \cdot \left(1 + \frac{k_s \zeta^2}{2\pi}\right) \quad (4)$$

$$\mathcal{E}_{max}(\zeta) = \mathcal{E}_{max0} \cdot \left(1 + \frac{k_s \zeta^2}{\pi}\right) \quad (5)$$

$$w = \frac{\mathcal{E}_i}{\mathcal{E}_{max}(\zeta)} \quad (6)$$

Where Vaughan later revised his equations by adding Equation 3 in [18] to account for behavior at large values of  $w$ . Such large values of  $w$  are unrealistic, however, in the course of numerical simulations, a few particles may reach such values and must be accounted for to assure stability of the code. Both simulations and calculations show

that most impact energies to fall primarily below the  $3.6\mathcal{E}_{max}$  threshold. This is best illustrated by Figure 3, where only a few particles rise above the  $3.6\mathcal{E}_{max0}$  line. Only when very small ( $\sim 5^\circ$ ) angles of obliqueness are introduced between  $E_{RF}$  and the dielectric surface do the impact energies move into higher values of  $w$ , a phenomenon which will be discussed in detail in Section 2.2.5.2.

Valfells, et al. [16] use the following continuous representation for  $k$ :

$$k = 0.435 - \frac{0.27}{\pi} \arctan \left( \pi \ln \left( \frac{\mathcal{E}_i}{\mathcal{E}_{max}(\zeta)} \right) \right) \quad (7)$$

In order to better understand and compare Vaughan's early and revised secondary equations with the continuous equation given by Valfells, et al. [16], Figure 4 plots the three different forms of the secondary emission yield for a material with a  $\delta_{max,0}$  of 3. This type of plot allows for an easier interpretation of the secondary emission function.  $\mathcal{E}_1$  and  $\mathcal{E}_2$  are commonly referred to as "crossover energies" and represent the impact energy at which the SEY is exactly one. When  $\mathcal{E}_1 \leq \mathcal{E}_i \leq \mathcal{E}_2$ , electron growth occurs within the system. As is evident from the piecewise definition of the equations, the plot may be broken up into three regions. The first region, which is shown in greater detail in the inset next to the main plot, describes the SEY of the material at low impact energies (less than  $\mathcal{E}_{max0}$ ). In this region, the first crossover energy,  $\mathcal{E}_1$ , is seen to differ by a relatively large amount when comparing Vaughan's early equations with the continuous form and Vaughan's revised equations. In the middle region, between  $\mathcal{E}_{max0}$  ( $\approx 750$  eV) and the vertical dashed red line (which corresponds to an approximate value of  $3.6\mathcal{E}_{max0}$ ), all the forms are seen to agree fairly well. In the region to the right of the  $\sim 3.6\mathcal{E}_{max0}$  line, the forms (especially Vaughan's revised form) diverge rapidly.

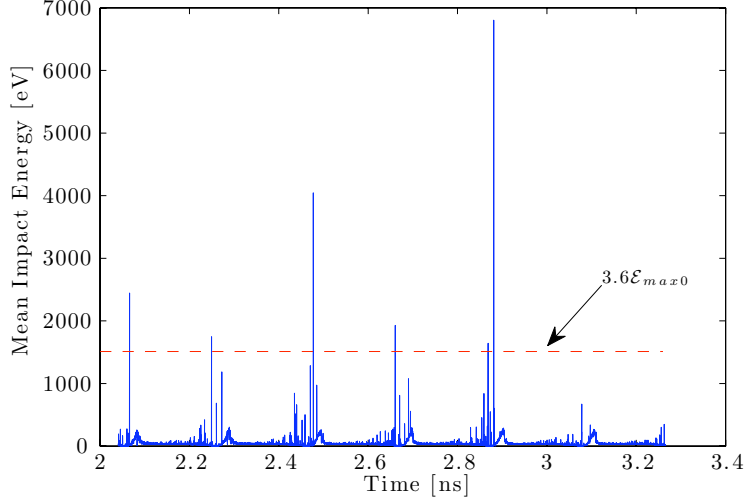


**Figure 3.** The mean impact energy of collected particles at discrete time steps is shown. In this system, space charge effects are considered and the following parameters are used:  $E_{RF} = 5.5$  MV/m,  $\delta_{max0} = 3$ ,  $\mathcal{E}_{max0} = 420$  eV,  $f = 2.45 \times 10^9$  GHz and  $k_s = 1$ . The dotted red line shows the impact energy which is equal to  $3.6\mathcal{E}_{max0}$ . From this figure, it is evident that very few particles obtain an energy requiring Equation 3, however, for these few cases, this additional region is imperative for numerical stability.

### 2.2.3 Kinematic Theory.

Using the relations of the impact energy and secondary emission (Equations 1 - 7), coupled with the equations of motion, the total energy gained by the electrons in flight may be determined, along with their flight time (also known as the "hoptime" of an electron) and the total power deposited on the dielectric by the electrons. The development and equations in this section are primarily from Valfells, et al. [16], where the equations have been slightly modified to match the conventions described in Section 2.2.1.

Beginning with the equations of motion, we can write the y-directed acceleration ( $a_y$ ) due to  $E_{RF}$  of an electron leaving the dielectric (such as one in Figure 5):

$$a_y = \frac{d^2y}{dt^2} = -\frac{eE_{RF}}{m} \sin(\omega t + \theta) = \frac{F_y}{m}$$

where  $\theta$  is the phase of the RF field at which the electron is emitted,  $F_y$  is the  $y$ -

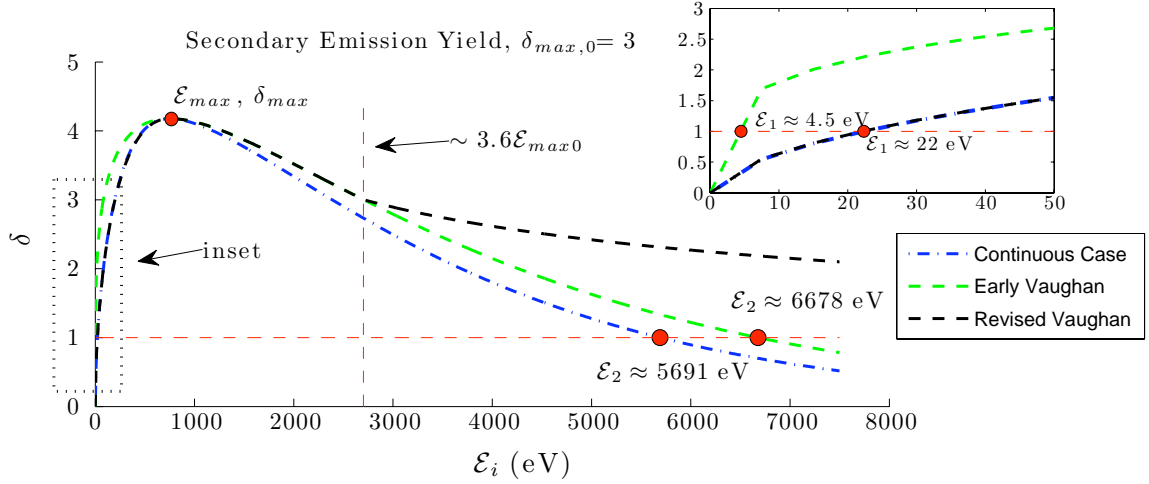


**Figure 4.** Comparison of the forms of the secondary emission equation. The horizontal dotted line shows the crossover point where  $\delta = 1$ , while the vertical dotted line shows the point at which  $\mathcal{E}_i \approx 3.6\mathcal{E}_{max0}$ .

directed force on the electron and  $e$  is the charge of the electron. Integrating once from 0 to  $\tau$ , where  $\tau$  is the hoptime of an electron, we obtain the  $y$ -directed velocity:

$$v_y = \frac{dy}{dt} = v_{0y} + \frac{eE_{RF}}{m\omega} (\cos(\omega\tau - \theta) - \cos(\theta)) \quad (8)$$

where  $v_{0y}$  is the  $y$ -component of the electron's emission velocity. Therefore, the energy gained by the electron during it's hoptime,  $\Delta\mathcal{E}_y$ , can be determined from

$$\Delta\mathcal{E}_y = \frac{1}{2}m\Delta v_y^2 = \frac{1}{2}m \left( \left( \frac{dy(\tau)}{dt} \right)^2 - v_{0y}^2 \right) \quad (9)$$

Substituting 8 into 9, we find:

$$\Delta\mathcal{E}_y = \frac{1}{2}m \left[ \left( v_{0y} + \frac{eE_{RF}}{m\omega} (\cos(\omega\tau - \theta) - \cos(\theta)) \right)^2 - v_{0y}^2 \right] \quad (10)$$

$$\begin{aligned} \Delta\mathcal{E}_y &= \frac{e^2 E_{RF}^2}{2m\omega^2} [\cos(\omega\tau + \theta) - \cos(\theta)]^2 \\ &\quad + \frac{v_{0y} e E_{RF}}{\omega} [\cos(\omega\tau + \theta) - \cos(\theta)] \end{aligned} \quad (11)$$

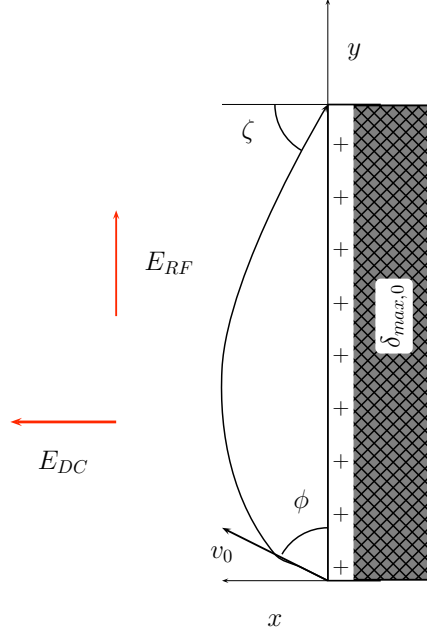


**Figure 5.** Figure 2 is shown again for convenience. The general geometry for single surface multipactor.

This impact energy is dependent on the phase,  $\theta$ , of  $E_{RF}$  at which the particle is emitted. Assuming a uniform emission distribution from 0 to  $2\pi$ , the following expression is found for the phase-averaged energy of a particle:

$$\langle \Delta \mathcal{E}_y \rangle_{\theta} = \frac{\int_0^{2\pi} \Delta \mathcal{E}_y d\theta}{2\pi} = \frac{e^2 E_{RF}^2}{m\omega^2} \sin\left(\frac{\omega\tau}{2}\right) = \frac{e^2 E_{RF}^2}{2m\omega^2} (1 - \cos(\omega\tau)) \quad (12)$$

This leaves the average energy as a function of  $\tau$ , the hop time. In order to obtain the total average energy, we now must average over the range of possible flight times:

$$\langle \Delta \mathcal{E}_y \rangle = \langle \mathcal{E}_0 \rangle + \int_0^{\infty} \frac{e^2 E_{RF}^2}{2m\omega^2} (1 - \cos(\omega\tau)) g(\tau) d\tau \quad (13)$$

Where  $g(\tau)$  is the distribution function of all possible flight times. The function  $g(\tau)$  is dependent on the distribution function of electron emission velocities, which is usually taken to be Maxwellian.  $\langle \mathcal{E}_0 \rangle$  is the average emission energy, which is also

dependent on the distribution function of electron emission velocities. Because space charge effects are included in this development, a solution to Poisson's equation is required:

$$\frac{\partial^2 \phi(x)}{\partial x^2} = \frac{en_0}{\epsilon_0} \exp\left(\frac{e\phi(x)}{kT}\right) \quad (14)$$

Where  $\phi$  is the potential of an electron density  $en_0$ ,  $n_0$  is the electron density at  $x = 0$  and  $\epsilon_0$  is the free-space permittivity. The number density profile is given by:

$$n(x) = \int_{v_{min}}^{\infty} \frac{v_0 f(v_0) dv_0}{v(x)^2}$$

where  $v_0$  is the injection velocity and:

$$\begin{aligned} v_{min} &= \sqrt{\frac{2e\phi(x)}{m}} \\ v(x)^2 &= v_0^2 + v_{min}^2 \\ f(v_0) &= \frac{2n_0}{\sqrt{\pi}v_t} \exp\left(-\frac{v_0^2}{v_t^2}\right) \end{aligned}$$

Using the Maxwellian distribution, the case-specific solution to 14 is:

$$\phi(x) = -\frac{E_0 v_t}{\omega_p} \ln\left(1 + \frac{\omega_p}{v_t} x\right) \quad (15)$$

where  $E_0$  is the surface electric field and  $\omega_p$  is the plasma frequency. These are given by:

$$E_0 = \sqrt{\frac{2kTn_0}{\epsilon_0}} \quad \text{and} \quad \omega_p = \sqrt{\frac{n_0 e^2}{m\epsilon_0}}$$

Which yields a number density,  $n(x)$ , profile of:

$$n(x) = \frac{n_0}{v_t} \exp\left(-\frac{2e\phi(x)}{mv_t^2}\right) = n_0 \left(1 + \frac{\omega_p}{v_t} x\right)^{-2} \quad (16)$$

Using the law of energy conservation, we can generate an equation describing the the motion of an electron in a potential given by 15:

$$v_x(t) = \frac{\partial x}{\partial t} = \sqrt{v_0^2 - 2v_t^2 \ln \left( 1 + \frac{\omega_p x}{v_t} \right)} \quad (17)$$

By setting the right hand side of this equation equal to zero, we can determine the maximum excursion of an electron, since  $x = 0$  describes the points at which the electron is at the dielectric surface:

$$\sqrt{v_0^2 - 2v_t^2 \ln \left( 1 + \frac{\omega_p x}{v_t} \right)} = 0 \Rightarrow x_{max} = \frac{v_t}{\omega_p} \left[ \exp \left( \frac{v_0^2}{2v_t^2} \right) - 1 \right] \quad (18)$$

At this point we can directly integrate 17 to determine the flight time for a given electron excursion in the potential of 15:

$$t = \sqrt{\frac{\pi}{2}} \frac{\exp \left( \frac{v_0^2}{2v_t^2} \right)}{\omega_p} \left[ \operatorname{erf} \left( \sqrt{\frac{v_0^2}{2v_t^2}} \right) - \operatorname{erf} \left( \sqrt{\frac{v_0^2}{2v_t^2} - \ln \left( 1 + \frac{\omega_p x}{v_t} \right)} \right) \right]$$

and, substituting in 18, we can determine the maximum flight time of an electron leaving the surface and returning to the surface after making an excursion of twice  $x_{max}$ . This is the hoptime referred to in 8-13.

$$\tau(v_0) = \sqrt{2\pi} \frac{\exp \left( \frac{v_0^2}{2v_t^2} \right) \operatorname{erf} \left( \sqrt{\frac{v_0^2}{2v_t^2}} \right)}{\omega_p}$$

Returning to 13, we can write:

$$\langle \Delta \mathcal{E}_y \rangle = \langle \varepsilon_0 \rangle + \frac{1}{n_0} \int_0^\infty \frac{e^2 E_{RF}^2}{2m\omega^2} (1 - \cos(\omega\tau(v_0))) f(v_0) d\tau$$

or:

$$\langle \Delta \mathcal{E}_y \rangle = \langle \varepsilon_0 \rangle + \int_0^\infty \frac{e^2 E_{RF}^2}{2m\omega^2} G\left(\frac{\omega}{\omega_p}\right)$$

Where  $y$  has been substituted for  $\frac{v_0^2}{v_t^2}$ , leading to:

$$G\left(\frac{\omega}{\omega_p}\right) = 1 - \frac{2\sqrt{2}}{\sqrt{\pi}} \int_0^\infty \cos\left(\sqrt{2\pi} \frac{\omega \exp(y^2) \operatorname{erf}(y)}{\omega_p}\right) \exp(-2y^2) dy \quad (19)$$

This describes the shielding effects in the system that arise from considering space charge effects. Now, we can determine the injection current density,  $J_0$ , for the Maxwellian distribution:

$$J_0 = e \int_0^\infty v f(v) dv = \frac{\sqrt{\pi} n_0 e v_t}{2} \quad (20)$$

From the impact energy and the current density, the power deposited on the dielectric is given by:

$$P = \frac{\langle \mathcal{E}_i \rangle J_0}{e} = \frac{\sqrt{\pi}}{4} \left[ 2\langle \varepsilon_0 \rangle \frac{m\epsilon_0}{e^2} \omega_p^2 v_t + \epsilon_0 v_t E_{RF}^2 \left(\frac{\omega_p}{\omega}\right)^2 G\left(\frac{\omega}{\omega_p}\right) \right] \quad (21)$$

Since space charge is an important part of the multipactor phenomenon, the previously discussed analysis includes these effects. According to Valfells, et al. [16], the main authority dealing with space charge effects, the power deposited can vary by up to a factor of 4 compared to when space charge is neglected. Many early research efforts, such as Kishek, et al. [12] ignored space charge effects; however, all recent research includes them in their analysis, since the effects have been experimentally and computationally demonstrated. The effects of incorporating space charge are evident when looking at Equation 16, since the number density,  $n$ , now varies spatially in the  $x$ -direction. This means that  $E_{DC}$  also varies spatially, hence the potential experienced by an electron is no longer constant.

While it has been determined that space charge is the dominant factor in multipactor saturation, the term "saturation" may be misleading. In fact, multipactor is a time-dependent phenomenon, as shown by Kim and Verboncoeur [9]. Since all work prior to this discovery relied heavily on time-averaged theoretical developments, the work was valid for that assumption and can be used as a guide in the time-varying case, as will be shown in Section 2.2.4. Kim and Verboncoeur [9] used simulation methods to show the amplitude of the electric field components and the number of electrons vary periodically over time. This has also been observed in execution of simulations [7] and a detailed comparison will be made in Chapter III.

#### 2.2.4 Interpretation and Characterization of Multipactor.

One of the most intuitive and useful ways to characterize multipactor is the susceptibility curve. Plots such as the one given in Figure 6 are commonly referred to as susceptibility curves. The lines on the plot represent the values of the RF field ( $E_{RF}$ ) versus the restoring field ( $E_{DC}$ ) for which the SEY is one. This particular susceptibility plot was created for several different values of  $\delta_{max,0}$ , which would represent different types of materials. The axes are scaled to  $f$  and  $\mathcal{E}_{max0}$ , so that the susceptibility curve varies only for values of the secondary emission coefficient; therefore, it is called "universal." In the region between the upper and lower curves, the SEY is greater than one; therefore multipactor occurs, resulting in an electron avalanche. When the corresponding values of the RF field and the restoring field fall in the region above the upper limit or below the lower limit, the SEY is less than one and results in total loss of particles back to the dielectric surface.

It is worth mentioning the conditions under which these susceptibility curves are generated through simulations. For all cases in which space charge is ignored, the value for  $E_{DC}$  is assumed to remain constant and multiple calculations are made with

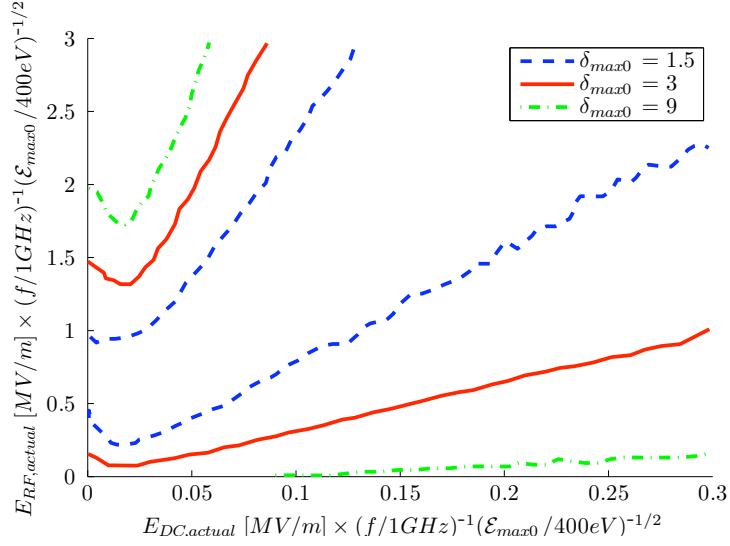


**Figure 6. Reproduction of Kishek’s universal susceptibility curves [12] for the simple (no space charge) case. The values are normalized to the frequency and  $\mathcal{E}_{max0}$ , hence, the term ”universal”.**

different values of  $E_{RF}$ . The pair of  $E_{DC} / E_{RF}$  values is then characterized based on a binary system (i.e., either multipactor growth occurred or it did not). Then,  $E_{DC}$  is changed and run against the same range of  $E_{RF}$  and the process repeated until the multipactor susceptibility regions are well-defined. This is a valid method, under the following two assumptions: that the hop time of an electron is short compared with the period of  $E_{RF}$  and  $E_{DC}$  does not change spatially (as the electron moves away from the surface). The latter is valid based solely on the non-space charge assumption.

Analytical expressions have been developed to describe these types of susceptibility curves by Kishek and Lau [11], as well as Semenov, et al. [14]. While the two forms of the boundaries are derived in different ways and yield seemingly different forms, there is good agreement on the boundaries. The two formulas for multipactor boundaries are examined below.

Kishek and Lau [11] give:

$$\frac{eE_{RF}}{\omega\sqrt{m\mathcal{E}_{max0}}} = \sqrt{\frac{2\mathcal{E}_c/\mathcal{E}_{max0}}{1 - \cos\left(\frac{4\omega\sqrt{m\mathcal{E}_{0m}}}{eE_{DC}}\right)}} \quad (22)$$

Where  $\mathcal{E}_{0m}$  is the peak value for the emission energy distribution of the electron,  $E_{RF}$  is simply the value for the RF field at the multipactor boundary (either upper or lower) and  $\mathcal{E}_c$  is the crossover energy associated with the same boundary. Sazontov and Semenov give

$$\begin{aligned} 2W_1/m < V_{RF}^2 < 2W_2/m & \quad \text{for weak DC fields} \\ (2W_1/mV_T^2)V_{DC}^2 < V_{RF}^2 < (2W_2/mV_T^2)V_{DC}^2 & \quad \text{for strong DC fields} \end{aligned} \quad (23)$$

Where  $V = \frac{eE}{m\omega}$  and  $W_1$  and  $W_2$  are the crossover energies. In order to compare the formulas, a few simplifying assumptions must be made. For example, in the case of a strong DC field, equation 22 becomes:

$$\frac{eE_{RF}}{\omega\sqrt{m\mathcal{E}_{max0}}} = \sqrt{\frac{2\mathcal{E}_c/\mathcal{E}_{max0}}{1 - \left[1 - \frac{1}{2}\left(\frac{4\omega\sqrt{m\mathcal{E}_{0m}}}{eE_{DC}}\right)^2\right]}} \quad (24)$$

which can be simplified to (after noting that  $\mathcal{E}_{0m} = kT$ ):

$$E_{RF} = \frac{E_{DC}}{2} \sqrt{\frac{\mathcal{E}_c}{kT}} \quad (25)$$

Similarly, noting that  $V_t = \sqrt{\frac{2kT}{m}}$  for strong DC fields, one side of the inequality in 23 becomes (using  $W_c$  to denote the crossover energy):

$$E_{RF} = \frac{E_{DC}}{\sqrt{3}} \sqrt{\frac{W_c}{kT}} \quad (26)$$

Thus, we see that 25 and 26 are nearly equal, within a small constant factor. Re-

ardless of this small constant factor, it is obvious that both confirm the dependence of  $E_{RF}$  on  $E_{DC}$ ,  $\mathcal{E}_1$ , and  $kT$ .

In his interpretation of the susceptibility curves, Ang [1] notes that, in contrast to the cavity (waveguide) case for which beam loading was the primary saturation mechanism, the primary mechanism leading to saturation of electrons in the case of a single dielectric surface is the growth of the  $E_{DC}$  field to a value for which the SEY is unity. He also notes that the amount of energy the multipactoring electrons absorb is a small, constant percentage of the total RF energy ( $\sim 1\%$ ). Although this may seem insignificant, in the case of HPM systems for which the power output is on the order of gigawatts, one percent of the RF energy would indeed be enough to cause failure in the dielectric window.

For the case in which space charge effects are included, the susceptibility curves (and interpretation thereof) change dramatically. Kim and Verboncoeur [9] reveal that a more accurate representation of the dynamics of a multipactoring system is given by Figure 7 and is referred to as the "bowtie" diagram for a given system.

In this case, the dotted lines are from the case in which space charge was ignored and serve as "guidelines" to denote the region in which multipactor occurs. These guidelines have been reflected around the  $E_{RF}=0$  line to show the complete variation of the RF field, instead of just the absolute value. The plot shows the trajectory of the system in susceptibility space ( $E_{RF}$  versus  $E_{DC}$ ) over time. The  $t = 0$  occurs at the point ( $E_{DC} = 0, E_{RF} = 0$ ) and as time progresses in the simulation the trajectory of the system follows the blue curve. The regions in which multipactor occur are between the top two red dotted lines and the bottom two dotted lines. Therefore, the values of  $E_{RF}$  and  $E_{DC}$  never reach a constant steady state, as was the case when space charge effects were neglected. Rather, they reach a periodic steady state, moving in and out of the multipactor region. As would be expected from this result,

the particle count also varies periodically (at a frequency of twice the period of  $E_{RF}$ ).

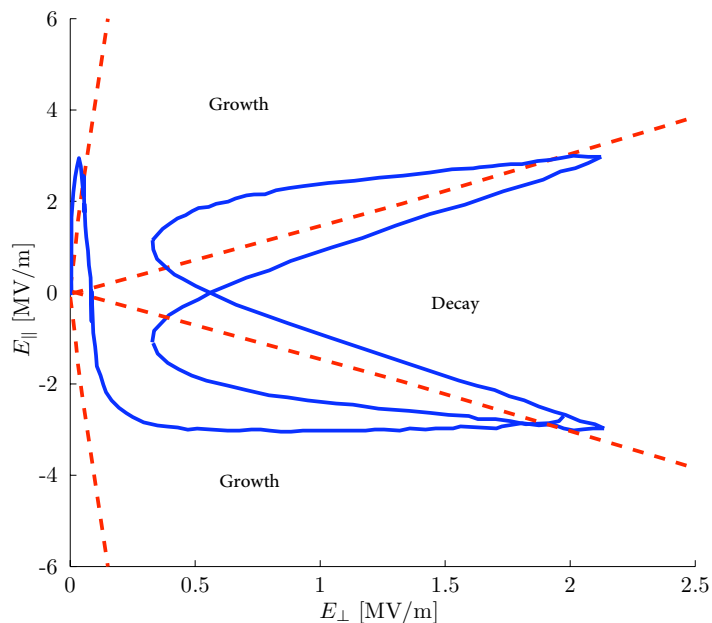


**Figure 7. Reproduction of Kim and Verboncoeur’s [9] periodic susceptibility curves or “bowtie” diagrams. Since this curve is not normalized, it varies for each set of parameters ( $E_{RF}$ ,  $f$ ,  $\delta_{max0}$ ,  $\mathcal{E}_{max0}$ ). The parameters for this plot are:  $E_{RF0} = 3$  MV/m,  $f = 1$  GHz,  $\delta_{max0} = 2$ ,  $\mathcal{E}_{max0} = 400$  eV. The dotted lines are “guidelines” from the case in which space charge effects were ignored.**

#### 2.2.4.1 Simulation.

Since experiments are extremely difficult and expensive to conduct, simulations are the most practical and widely used method of examining multipactor in HPM (and other) devices. A specific type of simulation code, known as Particle-in-Cell (PIC) code, is particularly useful, since it makes very few physical assumptions and lends itself to a quantitative analysis. In general, PIC codes follow the mathematical flow given in Figure 8, obtained from Barker [3].

The first major simplification PIC code introduces is to represent a large number of particles by a single macroparticle, which maintains the same charge to mass ratio as the original particle. In this way, the number of particles which the PIC code

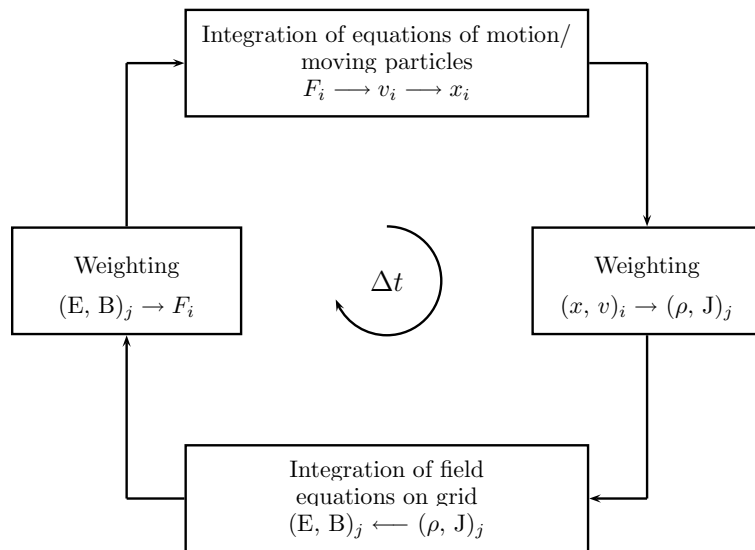


**Figure 8.** The general mathematical flow of PIC codes, as given by Birdsall [5].

must track and account for is inherently reduced. In Figure 8, the index  $i$  is used to reference quantities associated with individual particles and the index  $j$  is used to reference the nodes of the spatial grid. Therefore, the code starts by solving the equations of motion for each particle. Then, since the position of each particle is known exactly, the charge of each particle is weighted to the surrounding corners of the grid. Once this weighting process is complete for every particle, the total charge contained in the system can be represented by a charge density at each node,  $\rho_j$ , and a current density,  $J_j$ , between the nodes. At this point, the Fast Fourier Transform (FFT) is used to solve Maxwell's equations (specifically, Ampere's law and Faraday's law) for the corresponding electric and magnetic fields. These fields can then be weighted back to the original particle locations and the particles moved according to the force exerted on them by the electric field. Finally, the cycle is repeated as the simulation continues. The Improved Concurrent Electromagnetic Particle in-Cell (ICEPIC) [4] code is remarkable in its ability to self-consistently calculate and

model all the electromagnetic effects within a system, both internally generated by the particle interactions and externally imposed. In the course of this research, two dimensional simulations (with three dimensional velocity vectors) are run in order to maximize computational efficiency.

There are a few restrictions and conditions that apply to general PIC code. The Courant condition governs the time step ( $dt$ ) associated with the simulation. According to this condition, the time step depends on the size of the cell and the relevant velocity. In the case in which space charge is ignored, this velocity is  $v_t$ , the thermal velocity. However, in the space charge case, the relevant velocity is the speed of light,  $c_0$ , which is several orders of magnitude higher. This means that the grid must be considerably more refined (i.e. smaller and a greater number of cells) for the space charge case. Additionally, it is important, in order to take advantage of ICEPIC's concurrent electromagnetic capabilities, the cell dimension should be on the order of the Debye length. Multipactor is also a statistical phenomenon, therefore, for simulations to be statistically valid, each cell in the interaction space should contain 5-10 macroparticles.

Computational PIC tools, such as ICEPIC and XPDP [19], in conjunction with Monte-Carlo simulations are the predominant modeling codes used to verify analytical developments. While the development of the analytical theory is well documented by Kishek, et al. [10], Ang, et al. [1], Valfells, et al. [16], and Kim and Verboncoeur [9], the simulation parameters were not as thoroughly documented throughout the same literature. However, in general, the results agree well with the theory. According to Ang, et al. [1], typical parameters for simulations are:

$$\begin{aligned} \delta_{max0} &= 3, \mathcal{E}_{max0} = 420\text{eV}, \mathcal{E}_{0m} = 2.1\text{eV}, E_{RF0} = 3\text{MV/m} \\ f &= 2.45\text{GHz}, E_{DC0} = 10\text{V/m}, Z_0 = 377\Omega \end{aligned}$$

Using a Monte-Carlo simulation, Ang, et al. [1] were able to demonstrate that, after an initial (very short) transient period, parameters such as  $n(t)$ ,  $E_{DC}$ ,  $\delta(t)$ ,  $\mathcal{E}_i$ ,  $t$  and  $P_{dep}/P_{RF}$  settled into periodic steady state values near those that were predicted by analytical theory. This is consistent with later research demonstrated by Kim and Verboncoeur [9] and Fichtl [7].

Valfells, et al. [16] were also able to show good correlation with theoretical results, using the XPDP1 code. Fichtl [7] updated ICEPIC to include secondary emission effects, verifying the code by comparing it to theory. Discoveries made during the course of this research will be applied to update and correct Fichtl's ICEPIC SEE code.

### **2.2.5 Mitigation Methods.**

Mitigation of multipactor in HPM systems is one of great current interest among the leading experts in the field. Investigation of two promising mitigation methods is the primary aim of this paper: depositing a thin coating of low-SEY material on the dielectric window and geometrical modification of the dielectric window.

#### **2.2.5.1 Thin Coatings of Low-SEY Materials.**

Since the materials used to construct the dielectric window in a HPM system typically have  $\delta_{max0} \sim 2 - 3$ , one possible method of multipactor mitigation is to reduce the SEY by deposition of a thin, durable and low-SEY material on the surface of the dielectric. This accomplishes two objectives: the previously mentioned lowering of  $\delta_{max0}$  (and, consequently,  $\delta_{max}$ ) and the "squeezing in" of the crossover energies, so that the range of impact energies for which the SEY is greater than 1 is much smaller. Both of these effects are evident from Figure 9. Desirable properties for such a material include: 1) low SEY, 2) good thermal stability and 3) minimum attenuation

of  $E_{RF}$ , so that the film does not become yet another significant loss mechanism. According to Castañada, et al. [6] and Kennedy, et al. [8], the SEY of Titanium Nitride (Ti:N) is much lower than 2 and can even be deposited and processed in a manner that brings it near 1. Of course, this is an ideal situation, but such processing is very difficult and precise work; therefore, it must be accomplished carefully in pristine, vacuum conditions. If the real secondary emission curve for such a material were known, it would be easy to simulate. However, secondary emission curves are also very difficult to measure and require an elaborate apparatus, so we can currently only estimate the parameters of materials. As can be seen from Equations 1 - 5, the only parameters necessary to generate a secondary emission curve for a given material are  $\delta_{max,0}$  and  $\mathcal{E}_{max0}$  (since  $\zeta$  and  $k_s$  are usually assumed to remain constant). Then, using ICEPIC, simulations can be run to determine the susceptibility to multipactor of the new, coated system.

### 2.2.5.2 Geometrical Modification of the Waveguide/Window Interface.

Modifying the geometry of the interface of the dielectric window with the waveguide means, in the simplest case, introducing a non-zero angle of incidence between the window and  $E_{RF}$ . This is equivalent to the window no longer being perpendicular to the waveguide, but offset by the angle  $\psi$ . With regard to RF field oblique orientation, Valfells, et al. [15] begin with the fact that the electron flight time is the most important factor in determining the susceptibility of a system to multipactor damage. In general, the longer an electron is in flight, the more energy it gains from the RF field and the more energy it possesses when it returns to the surface. An oblique RF field angle of incidence, introduces a component of  $E_{RF}$  in the direction of  $E_{DC}$  and can either enhance or degrade the time of flight of electrons, thereby in-

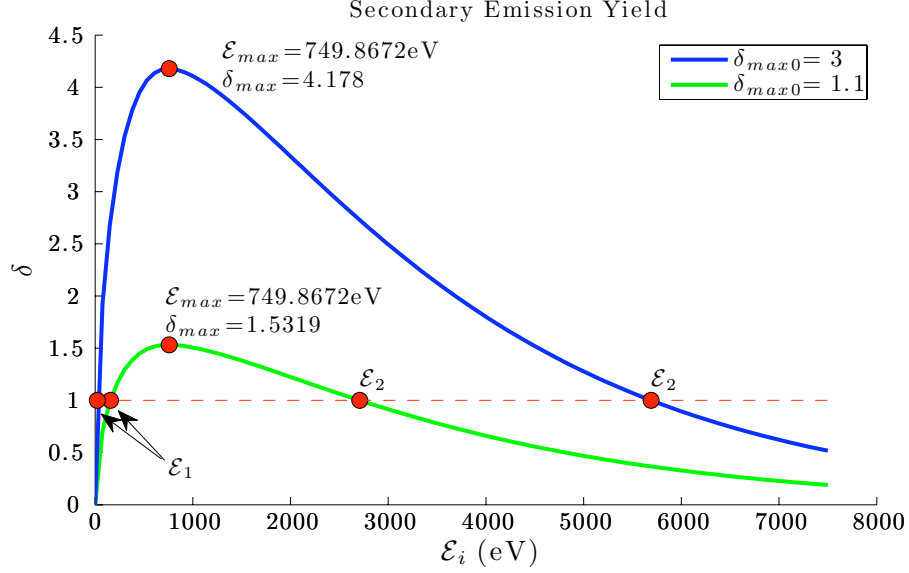


**Figure 9.** A comparison of secondary emission yield curves. The only parameter varied in this plot is  $\delta_{max0}$ , showing the drastic difference a reduction in this material parameter can make.

creasing or decreasing the susceptibility of the system to multipactor. Such a system is one in which  $\psi$  in Figure 10 is greater than zero. According to Valfells, et al. [15], for  $\psi < \sim 5^\circ$ , the susceptibility curve is widened; however, larger values of  $\psi$  result in a considerably narrower susceptibility curve.

Formulas for the trajectories and flight times of electrons in a system with an obliquely incident RF field are given by Valfells, et al. [15]:

$$v_x = v_0 \sin(\phi) - E_{DC}t + E_{RF0} \sin(\psi) (\cos(t + \theta) - \cos(\theta)) \quad (27)$$

$$v_y = v_0 \cos(\phi) + E_{RF0} \cos(\psi) (\cos(t + \theta) - \cos(\theta)) \quad (28)$$

$$0 = (v_0 \sin(\phi) - E_{RF0} \sin(\psi) \cos(\theta)) T - \frac{E_{DC}}{2} T^2 + E_{RF0} \sin(\psi) (\sin(T + \theta) - \sin(\theta)) \quad (29)$$

Formulas 27 - 29 can be used to calculate the energy of an electron returning to the surface using the elementary relationship  $1/2 (v_x^2 + v_y^2)$  [Note: The mass of the

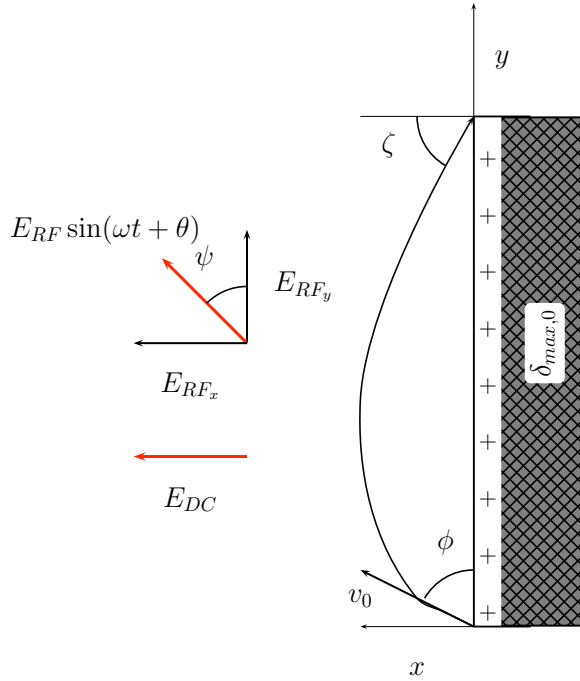


**Figure 10.** The geometry for single surface multipactor. This is the same as Figure 2, except an angle of incidence,  $\psi$ , has now been introduced between the surface and  $E_{RF}$ . This is equivalent to placing the window at some angle  $\psi$  off of normal to the waveguide.

electron has been normalized out of this set of equations.] Valfells, et al. [15], use simulations to obtain the susceptibility curves for the oblique incidence case. These simulations revealed that for values of  $\psi < 5 - 10^\circ$ , the susceptibility curve is broadened, but for larger values of  $\psi$ , the region of susceptibility to multipactor is drastically reduced. The reason for the broadening at small angles of obliqueness is related to the slope of the secondary emission curve at the lower boundary. Figure 11 shows the SEY plotted as a function of the restoring field ( $E_{DC}$ ), rather than the impact energy. The higher restoring field is related to the lower boundary on the susceptibility curve (which is the first crossover energy,  $\mathcal{E}_1$ ). When a component of  $E_{RF}$  exists in the direction of the  $E_{DC}$ , the restoring field can now be either slightly smaller or slightly larger, depending on the phase of the RF field. Because the slope is decreas-

ing near this point, denoted by the lower boundary label in Figure 11, the *average* secondary emission due to this small change in the restoring field would be higher than for the restoring field by itself. For larger angles of obliqueness, the RF field component in the direction of the restoring field generally decreases the restoring field by a greater amount, resulting in a longer flight time and electrons returning to the dielectric surface with more energy, such that the SEY becomes less than one. This effect dominates over the previously discussed change in the restoring field. Thus, the susceptibility region will be significantly diminished for larger angles of obliqueness. An analytical method which utilizes MATLAB to examine the change in the susceptibility curves is described in detail in Chapter III and the results compared with Valfells' in Chapter IV.

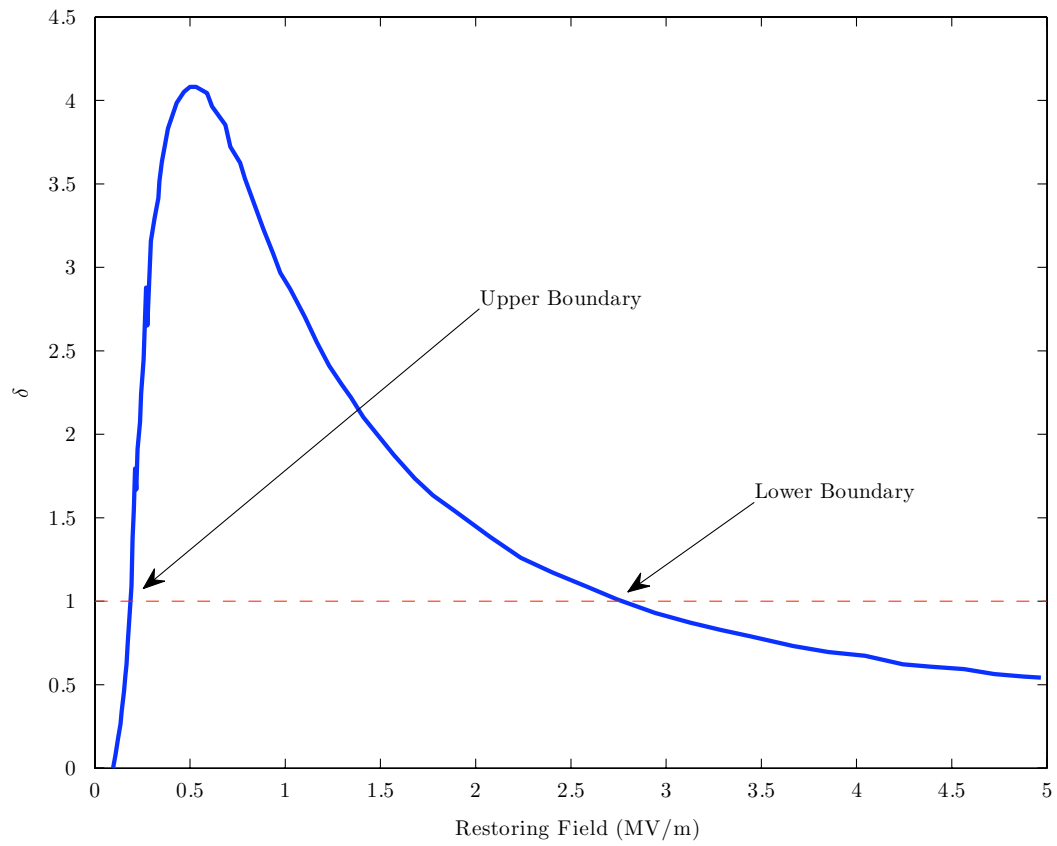


Figure 11. Secondary emission curve as given by Valfells, et al. [15]

### III. Computational Models and Comparison with Theory

This chapter describes the rationale behind the selection of ICEPIC input parameters, including assumptions made in running simulations. This is followed by a detailed description of basic simulations that were run in order to verify our system by comparing the results with the theory described Kishek, et al. [10], Ang, et al. [1], Valfells, et al. [16] and Kim and Verboncoeur [16]. Also, the numerical and simulation models for potential mitigation methods are thoroughly described.

#### 3.1 ICEPIC Input Parameters

This section includes a detailed discussion and explanation of the input parameters used in simulating the cases follows, broken up into functional sections. While a nominal understanding of the operation of ICEPIC is necessary to completely grasp the complexity of the system, a general understanding of PIC code will suffice when reviewing the following discussion. ICEPIC simulations are controlled by input files, which contain parameters that allow a wide variety of physical phenomena to be simulated. This section will describe each section used in generating the simulations used throughout the course of our research, explaining the purpose of the most important parameters. As a matter of convention, each functional section in the input file is denoted by a title enclosed in square brackets - i.e, the first section is the [Defaults] section. Also, comments are denoted by a semicolon, such that everything from the semicolon to the end of the current line is ignored by the code. When running an input file, ICEPIC considers the entire file and is not, for the most part, sensitive to the order in which sections are entered. The complete input files for both the NSC case and the SC case can be found in Appendices A and B. For a complete explanation of every available parameter and section, please see the ICEPIC User's

Manual [4].

### 3.1.1 Defaults and Variables.

The [Defaults] and [Variables] sections allow a user the ability to define variables for easy reference and usage throughout the rest of the input file. The difference between the two sections is that variables placed in the [Defaults] section are eligible for parametric surveys. In this case, a separate script can be used to generate many input files containing a survey of values for a particular variable. As an example, the input files given in Appendix A contains the ENERGY variable, which is later used to assign the value of  $E_{RF}$  (for the NSC case). In building the surveys that were used to create the lower multipactor boundary, a script was run to generate many input files containing a range of values of for both  $E_{RF}$  and  $E_{DC}$ .

### 3.1.2 [Time] Section.

The [Time] section contains parameters that pertain to the simulation time, including:

- **dt** - This is the fundamental time step, of the simulation.
- **step\_max** - This represents the total time for the simulation, in units of number of **dt** steps.
- **courant\_value** - This is a constant value which determines what the time step should be set to should the Courant condition not be satisfied.
- **kill\_if\_below\_parts** - Once the number of particles in the system reaches this minimum value, the simulation is terminated.
- **kill\_if\_above\_parts** - Once the number of particles in the system reaches this maximum value, the simulation is terminated.

### 3.1.3 System Geometry.

The system geometry is defined in many different sections of the input file, specifically:

- [Cartesian] - Setting `ig_dir` to (0,1,0) causes the code to physically ignore the  $y$  direction, making this a two-dimensional survey. In the NSC case,  $E_{DC}$  is set by the `default_e` parameter.
- [XGrid1], [YGrid1], [ZGrid1] - These three parameters define the computational grid for the simulation, including the physical extent, the size of the cells,  $dx$ ,  $dy$  and  $dz$ , and the number of cells in each direction,  $N_x$ ,  $N_y$  and  $N_z$ .
- [Symmetry] - Sets the periodic boundary conditions for the system.
- [ShapeN] - These sections define physical shapes in the computational domain. The initial domain is considered to be a metallic cube and the physical shapes are "carved" out of this cube using a number of [ShapeN] sections. The sections are numbered during the pre-simulation processing script. The physical properties of the shape are determined by the `material` parameter, which may be more specifically defined in the [MaterialN] section.
- [MaterialN] - The physical properties of the shapes may be defined and referenced by assigning a name to any number of materials. Similar to the [ShapeN] sections, these sections are numbered during the pre-simulation processing.
- [BoundN] - Boundary conditions may be set using these sections. For the purposes of this research, a Perfectly Matched Layer (PML) boundary condition is employed.

Figure 12 shows the geometrical configuration of the system used during these simulations, which is generated by the above sections. This is very similar to the geometries

used in previous work by Fichtl [7] and Verboncoeur, et al. [9]. In this configuration, the physical size of the system scales with the wavelength in any direction. The dielectric material is given a default  $\epsilon_0$  of 1.001, so that, in the electromagnetic sense, it simulates a nearly opaque material, allowing the RF energy to propagate with no significant attenuation. This is, naturally, a realistic assumption for HPM systems. The purpose of the dielectric on the left side of the system is to shield the plane wave emitter from any particles that may traverse the length of the system. For the parameters given in Section 2.2.4.1, typical values for the SC case would be (for  $Nx = 3$  and  $Nz = 500$ ):

$$\begin{aligned}
 dz &= \frac{\lambda}{12000} \\
 \Delta x_{SC} &= Nx \times dz = \frac{(3)(0.122\text{m})}{12000} \approx 3.05 \times 10^{-5} \text{ m} \\
 \Delta z_{SC} &= Nz \times dz = \frac{156 \times 0.122\text{m}}{12000} \approx 1.6 \times 10^{-3} \text{ m}
 \end{aligned}$$

In order to fulfill the condition that there must be many particles contained in a Debye sphere when considering individual particle interactions,  $dz$  for the SC case is four times smaller than  $dz$  for the NSC case, therefore the dimensions for the NSC case are four times larger than those in the SC case.

A PML enforces the electromagnetic boundary conditions behind the dielectric and prevents any backscattered waves from affecting the simulation by introducing layers of successively higher conductivity. The system is symmetrical (or periodic) in the  $x$ -direction, so that any particle leaving the system in on one side of the system at  $x_{max}$  reenters the system at  $x_{min}$  and vice-versa.

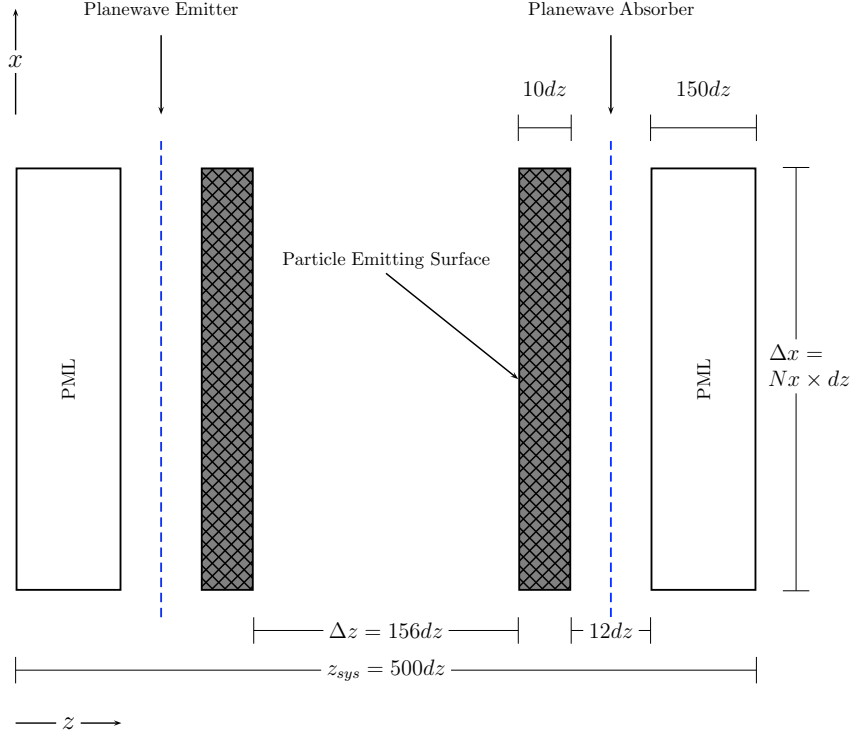


**Figure 12.** The geometry used for ICEPIC simulations.  $N_x$  and  $N_z$  are the number of cells in the respective direction,  $dz = \lambda/3000$  is the width of a cell. The particle emitter, planewave emitter and planewave absorber take up no physical space.

### 3.1.4 Plane Wave Emission.

$E_{RF}$  is simulated by a plane wave that extends across the system in the  $x$ -direction, originates from a plane behind the left hand dielectric and propagates in the positive  $z$ -direction, as shown in Figure 12. In the input file, this is created by the [PlanewaveN] section. The ICEPIC code actually creates a plane wave emitter on one side of the system and a plane wave absorber on the other side of the system, for computational stability. This is reflected in the definition of the `shape` parameter in this section.

The magnitude of  $E_{RF}$  is determined by the E0 parameter, which is set by the `energy` variable, which is assigned a default value in the [Defaults] section by ENERGY. The frequency of the system is taken to be that of the RF field. For the NSC

case, the restoring field ( $E_{DC}$ ) is set in the [Cartesian] section by the `ez` variable, which is also assigned a default value in the [Defaults] section by `EDC`. This same methodology is used to create a time-varying E-field in the case of the geometrical modification mitigation method (the specific implementation is discussed in Section 3.3).

### 3.1.5 Particle Emission.

Particle emission is generated in the ICEPIC input file in the [ParticlesN] sections. Two main variants of this section are used through the course of this research:

- Primary particle emitter - This section provides seed particles to the system and is defined by setting `method` to `BEAM`. The parameters that control the beam emission are:
  - `temp` - Controls the initial temperature of the injected particles.
  - `inject_interval` - Determines the injection frequency of the particles and is given in units of  $dt$ .
  - `current` - One of the main factors in determining the macroparticle weighting - which is, in this case, is fully described by:  $\frac{\text{current} \times dt}{\text{inject}}$ , where `inject` is the number of particles emitted per emitting face (where each  $Nx$  is an emitting face) per time step and, for this case, is 1.
  - `tstop` - Determines the time at which particle injection ceases, in this case particles are injected for half an RF period.
  - The other parameters contained in this section are used to smooth out the emission waveform and probably may be omitted.
- Secondary particle emitter - This section, specified by setting `method` to `SECONDARY`, defines the secondary emission properties of the dielectric face, per the sec-

ondary emission equations given in Section 2.2.2. The parameters that control the secondary emission properties are:

- `sec_coefficient` - Corresponds to  $\delta_{max0}$ .
- `sec_energy` - Represents the average emission energy of secondary particles.
- `sec_refl` - The fraction of secondary electrons that are reflected from the surface of the dielectric.
- `sec_scatt` - The fraction of secondary electrons that are scattered from the surface of the dielectric.
- `sec_energy_max_yield` - Corresponds to  $\mathcal{E}_{max0}$ .
- `sec_ks` - The smoothing constant, related to the surface smoothness of the material.

In each section, the properties of the particles are defined by the `mass` and `q` (charge) parameters. The `dir` parameter defines the direction in which the particles are emitted. Also, the `shape` parameter defines the plane face from which the particles will be emitted.

The particle emitter and secondary emitter are created by very narrow (about half a cell wide), non-physical faces on the surface of the right hand dielectric. The primary particle emitter section is used to provide a small amount of seed current to the system. [NOTE: in ICEPIC, the `current` parameter is one of the parameters used to determine the macroparticle weighting, that is, how much charge each macroparticle carries.] This current is large enough to provide seed electrons to the system, but not so large as to affect whether or not the system is operating in a multipactoring region or to produce an electron density that is too high (such that a large amount of power is reflected back towards the source). Also, the current is only injected for half an

RF period, so that it will not interfere with the amount of energy measured in the particles or the power of the system. The particles are injected with a Maxwellian distribution of velocities, given by:

$$f(v_0) = \frac{2n_0}{\sqrt{\pi}v_t} \exp\left(\frac{-v_0^2}{v_t^2}\right)$$

where  $v_t = \sqrt{\frac{2kT}{m}}$ , therefore the energy of the seed electrons is specified by a particular temperature,  $T$ , which is the parameter `temp` in the primary particle emitter section of the ICEPIC input file. The length of time for the seed period is one-half of an RF period, so as to inject particles at many phases of the RF field. In this case, the particles are injected with a frequency of 30 times per RF period.

Several simulations were run to determine the most efficient way to control particle weighting and, effectively, the run time of the simulation. It was found that, for a constant emitting area, that maintaining the default injection rate of 1 macroparticle per  $nx$  per  $dt$  and increasing the injection current results in a proportional increase in the macroparticle charge. This further results in a decreased number of particles in the system, higher computational efficiency and strikingly comparable results. This does not cause any distortion of the results because the macroparticle charge to electron charge ratio is always accounted for in the post-simulation analysis of data. However, for the case in which  $E_{RF} = 5.5$  MV/m, this resulted in a run-time savings of almost 40 hours, since ICEPIC run time increases nearly exponentially with the amount of particles in the system. The most important factor to consider is to make sure that the critical electron density is not exceeded, such that the reflected power is not too high. The critical electron density is the high electron density at which total reflection of incoming power occurs and is discussed in further detail in Section 4.1.2. Also, enough macroparticles must be present, so as to produce a statistically valid answer. Typically, this is on the order of a few macroparticles per cell over the interaction

space. Therefore, determining the appropriate macroparticle weighting is a delicate balancing act and must be carefully considered when running PIC simulations.

The secondary emitter surface models the secondary emission, as described by Vaughn [17]. The energy of the emitted secondaries is also determined by a Maxwellian distribution and is specified by the parameters in the `[ParticlesN]` section denoted by `method=SECONDARY`. Scattering and reflection effects are also included for all simulation and analyses, per Fichtl [7], except where otherwise specifically noted.

### 3.1.6 Dump Parameters.

In ICEPIC, many different quantities may be written to output files, or "dumped" throughout the course of a given simulation, using the `[DumpN]` sections. The quantities may be dumped over the whole simulation or during any specified part of it. Specific dumps are created by setting `method` to the dump name. As with other sections, the `[DumpN]` sections are numbered during the pre-simulation processing scripts. While some of the dump sections in the sample input files are commented out, the most useful sections are described below:

- **FIELD** - This dumps the vector electric and magnetic field quantities at every node in the specified volume. In the course of this research, the RF field taken to be the  $x$ -directed component and the restoring field is taken to be the  $z$ -directed component.
- **POWER** - The Poynting flux through the plane specified by the `dump_value` parameter is dumped. This represents a power density and can easily be converted to power using the system geometry.
- **PART** - This dumps out the position, velocity and charge for every particle in the specified volume. Since the number of particles in a simulation can become very

large, these dump files can become quite large and should be used sparingly. The `PART` dump also allows for only information about particles collected at any boundary in the system to be written, which drastically reduces the size of the files and allows calculation of the power deposited on the surface of the dielectric window, as described in Section 3.2.3.

Every dump parameter may be controlled by a common set of parameters, including:

- `dump_int` - Determines how frequently dump files are created.
- `nstart` - Sets the starting time for the dump files, in units of  $dt$ .
- `nstop` - Sets the stop time for the dump files, in units of  $dt$ .

### 3.1.7 The [Expert] Section.

The [Expert] section contains two vital parameters used through in performing these simulations:

- `requested_max_num_particles` - Once the simulation reaches the number of particles specified by this parameter, the weighting of particles emitted by the secondary emission code will be increased instead of emitting more than one particle. This is one way to maximize computational efficiency, but makes post-simulation analysis of particles much more difficult, due to the many different weightings that may be present in the system.
- `self_fields` - This parameter determines whether or not space charge effects are included. If set to 0, ICEPIC simulates the NSC case, such that the particles only move under the influence of external fields. If set to 1, the current density of the particles is incorporated in the solution of Maxwell's equations.

### 3.1.8 ICEPIC Code Updates.

In the process of verifying previous results, updates to ICEPIC code were necessitated. While this is by no means a complete listing of updates made to the code during the period in which this research was performed, this section contains a short description of some of main code updates that were required through the course of this research.

1. **DENSITY Dump** - It was discovered that this particular dump contains an error and produces no output when running on a multi-processor machine. This error did not affect the scope of our research; however, the **DENSITY** dump is an extremely useful dump, containing (for each cell and dump interval): real particle number density, velocity information, energy information and the number of macroparticles.
2. **POWER dump unit conversion** - A factor of 100 reduction is present in the **POWER** dump file values. This unit conversion comes from the internal dimension for the ignorable direction (in this case,  $y$ ) being set to 1 cm rather than 1 m in a two dimensional simulation.
3. **PART dump unit conversion** - A factor of 100 was found in the charge column of the dump file, when `collected_part=1`. The values reported in this research have been compensated for this factor.
4. **Surface Normal Error** - The general particle emission code was passing an incorrect cell normal direction to the secondary electron emission code, which was then using that value to determine emission and reflection angles for reflection and scattering of secondary electrons. This bug was fixed in the version of ICEPIC used for this work.

The input files used in the course of this research were based on those presented by Fichtl in [7], however, several parameters in Fichtl’s input files were no longer supported by the ICEPIC code. These parameters were:

1. `symmetry`, `sym_mode` in the [Symmetry] section - These legacy parameters were replaced with the updated `periodic` parameters.
2. `cell_mult` in the [Expert] section - No documentation was found for this parameter, so it was removed from the code. Apparently, it was a correction factor for a known issue in ICEPIC, which has been fixed.
3. [ShapeN] sections - An adjustable buffer, called `zbuff`, was introduced in the `SHAPE` sections in the  $z$ -direction on both sides of the Plane Wave Emitter/Absorber (on both ends of the system), in order to investigate the effects of the size of such a buffer on `POWER` and `FIELD` dumps. It was thought that several cells on either side of the Plane Wave Emitter/Absorber allowed more room for the `FIELD` and `POWER` dumps and left less potential for instabilities caused by the proximity of the boundaries to the dump planes. However, very little difference was found when introducing a  $6dz$  wide buffer versus the  $1dz$  buffer used by Fichtl.

## 3.2 Comparison of Results

### 3.2.1 Non-Space Charge (NSC) Case.

The NSC case, in which space charge effects are ignored, is the simplest case and the most rational starting point for a verification of multipactor theory in ICEPIC. Most of the theory from this section will be compared with Fichtl’s [7] results. In this case, the electromagnetic contributions of particles are ignored (meaning that the current density is not updated in Maxwell’s equations) and only the fields imposed by

external sources are considered. Thus, it is necessary to specify a constant value for  $E_{DC}$  in order to facilitate multipactor growth. Using the same methodology Fichtl [7] uses (which is described in Section 2.2.4), the lower multipactor boundaries in Figure 13 were reproduced. The upper boundary is not considered, because, according to Barker [3], the lower boundary is associated with saturation. In this case, the only metric used to determine multipactor growth was whether or not the number of particles in the system grows significantly beyond the initial seed particles. In order to maximize computational efficiency, the simulations are terminated if they reach a maximum number, specified by the `kill_if_above` parameter in the [Time] section of the input file in . This number is well above the number of particles necessary to qualify a particular simulation for multipactor growth. One notable variation between the results is the fact that the boundaries do not match up exactly. This is most likely due to updates to the secondary emission code within ICEPIC since Fichtl performed his research. However, the correlation of the curves is satisfactory and confirms the simulations were appropriately configured. This process could be repeated for different secondary emission coefficients, however, these types of surveys are time consuming and it is assumed that this result implies that other surveys would demonstrate similar behavior.

In order to demonstrate the rapidly evolving nature of multipactor, Figure 14 shows the particle growth in regions near the lower susceptibility boundary. From these figures, it is evident that multipactor growth occurs very quickly - usually within a few nanoseconds (where the period of the RF cycle is 0.4 ns and a hoptime may be on the order of 1 ps). These points at which these plots are generated are different from those in Figure 8 of [7], because they have been adjusted to correspond to the susceptibility curves generated by more current simulations (i.e. those shown in Figure 13).

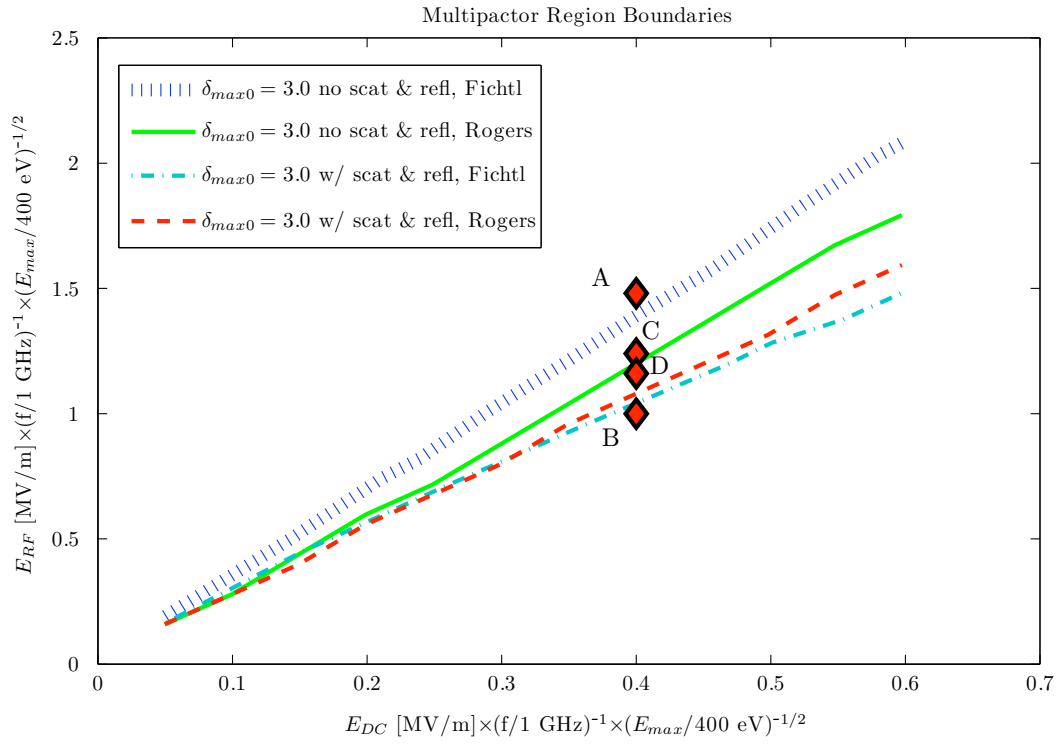
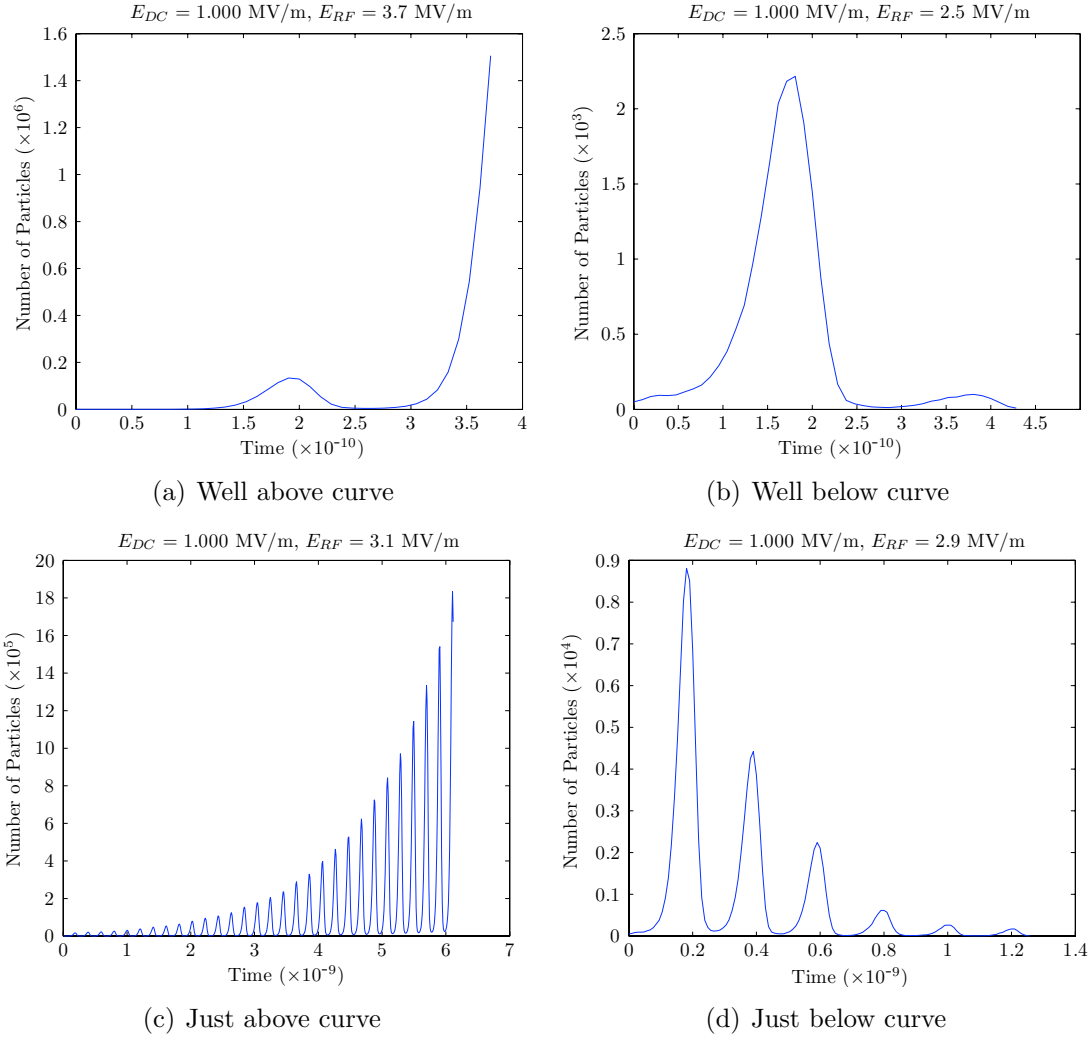


Figure 13. Comparison with Fichtl's multipactor boundary curves. The labeled points correspond with the points selected for Figure 14 and are in reference to the Rogers case with no scattering or reflection effects (solid green line).



**Figure 14.** Particle growth for points near the lower multipactor boundary curve. In this case,  $f = 2.45$  GHz. Each of these points is shown on Figure 13

### 3.2.2 Space Charge Case.

In the previous case, space-charge effects were ignored. While this is a good guide to what may happen in an actual system, including the contributions of electrons to the restoring field during the multipactor process provides for a more realistic simulation. In this case,  $E_{DC}$  is not constant, but changes both temporally and spatially, since the electron density also varies in time and space. Valfells, et al. [16], examine the effects of the spatial variation by using a time-averaged model. Through this model, they conclude that the percentage of input power deposited on the surface for the case when space-charge effects are included is no longer a fixed percentage of the input power (as was determined to be the case by Ang, et al. in [1]), but the percentage of power deposited varies based on the magnitude of  $E_{RF}$ . This result is confirmed by Fichtl [7].

In comparing our simulations with theory in the case where space-charge effects are taken into account, it is more useful to compare with the results presented by Valfells, et al., [16] and Kim and Verboncoeur [9] than with those presented by Fichtl [7], since Fichtl creates susceptibility curves based on time-averaged values of  $E_{DC}$ . While, again, this is a useful guide as to when multipactor occurs in a system, it does not fully represent the actual physics of the multipactor phenomenon.

First, it is useful to look at the time-variant physics of the problem as presented in Verboncoeur, et al. [9]. As is shown in Figure 15, the restoring field,  $E_{DC}$ , varies periodically in time, as does the number of particles in the system. As was alluded to in Figure 7, the plot of  $E_{DC}$  versus  $E_{RF}$  is no longer a straight line. Instead, the result is a parametric plot of  $E_{DC}(t)$  and  $E_{RF}(t)$ , describing the system trajectory in susceptibility space through the simulation. This is referred to as a "bowtie" plot. Thus, as the system settles into a periodic steady state, the values of  $E_{RF}$  and  $E_{DC}$  are shown to move along the periodic curves shown in Figure 16. The dotted lines are

created by the "simple" theory (the case in which space-charge effects are ignored) and are reflected around the  $E_{RF} = 0$  line to show the positive and negative values of  $E_{RF}$ , rather than just the absolute value. When the trace is between the two upper and two lower dotted lines, electron growth due to multipactor occurs; however, when it is between the two middle dotted lines, the number of electrons in the system decays. Since the "bowtie" plot shows the system trajectory moving periodically through regions of electron density growth and decay, it can be reasonably expected from these plots, therefore, that the electron density changes in a periodic manner. The plots in Figure 16 were generated using the same parameters given by Valfells, which are listed in Table 1. Consequently, these plots also confirm Barker's assertion in [3] that the lower boundary, not the upper boundary, is associated with saturation in the system, since the traces circulate around the lower boundaries. This further justifies consideration of only the lower boundary.

Valfells specifies a seed current of  $J_{init} = 1.3 \text{ kA/m}^2$ , however he concludes that the seed current is in fact irrelevant in the final, steady state of the system. This is true, for the most part, unless the critical electron density described in Section 4.1.2 is reached, in which case total reflection of the input power occurs. Additionally, since the times for which dumps are made are considerably longer than the seeding time, the seed current does not greatly affect the results of the simulations. In fact, the effect of increasing the seed current is equivalent to increasing the macroparticle

**Table 1. Parameters from Kim and Verboncoeur [9] used to verify ICEPIC simulation setup**

$\delta_{max0}$	2
$\mathcal{E}_{max0}$	400 eV
$k_s$	1
$T$	2 eV

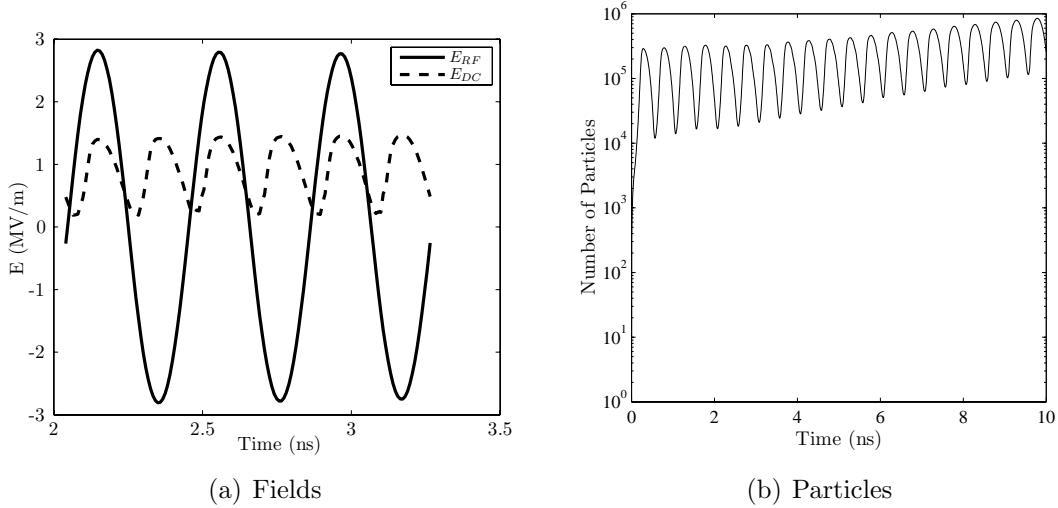
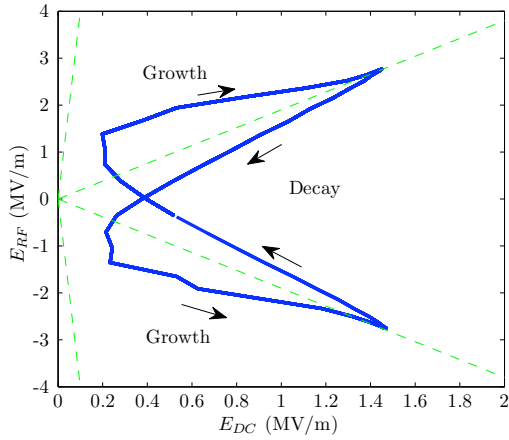


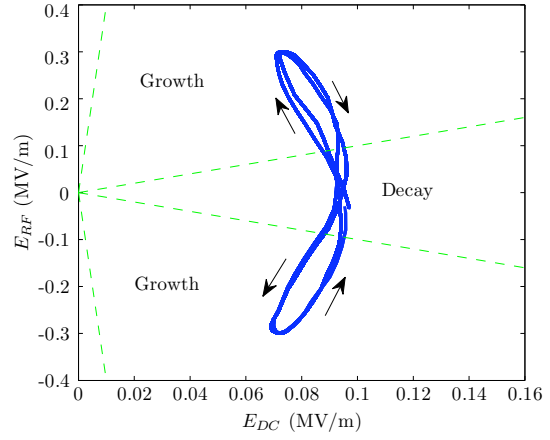
**Figure 15. Evolution in time of fields and particles in a multipactoring system, with  $E_{RF} = 3$  MV/m and  $f = 1$  GHz. Note that the fields are only shown for a small portion of the entire simulation, but the particle count represents the simulation in its entirety.**

weighting and decreasing the total number of macroparticles in the system. Therefore, we use a considerably larger seed current, in order to shorten the time needed to run the simulations.

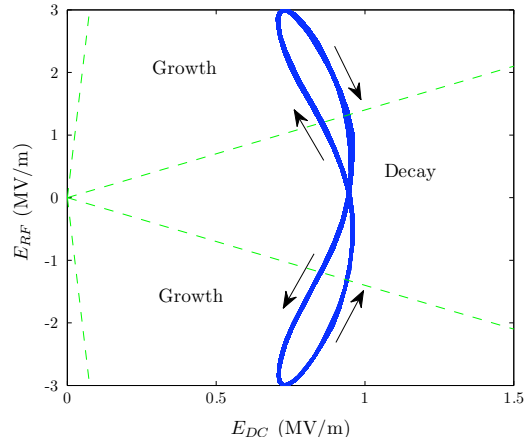
Figure 16 confirms the simulations and theory published by Kim and Verboncoeur [9]. The shape of these diagrams correspond very well with those given in those results, however, they do not align exactly with Kim and Verboncoeur’s simulations. This is most likely due to three factors: lack of complete knowledge of initial parameters (such as particle weighting and system geometry); inclusion of scattering and reflection effects in the most recent simulations; and fundamental differences in the ICEPIC code (since it self-consistently calculates all the Electro-Magnetic (EM) fields in the system). All of the simulations with space-charge effects included demonstrated similar behavior, thereby confirming the validity of our input file.



(a)  $E_{RF} = 3$  MV/m,  $f = 1$  GHz



(b)  $E_{RF} = 0.3$  MV/m,  $f = 1$  GHz



(c)  $E_{RF} = 3$  MV/m,  $f = 10$  GHz

Figure 16. Results of the simulations detailed by Kim and Verboncoeur [9]. These curves detail the evolution of  $E_{RF}$  and  $E_{DC}$  in time, representing a periodic steady state. The arrows show the direction of the system trajectory and the areas of electron density growth and decay are labeled.

### 3.2.3 Power Deposition on the Dielectric Surface.

For the NSC case, it is determined by Ang [1], that the percentage of power deposited on a dielectric surface is a fixed fraction of the input power ( $\sim 1\%$ ). However, as is shown by Valefells, et al. [16], this is not the case when space charge effects are considered. According to Fichtl, in [7], although "the power deposited is no longer on the order of 1 % as is initially estimated, we find that it is generally less than 5 % regardless of the input parameters." This section will examine three different methods in which attempts were made to verify Fichtl's numerical results and a table of comparative values is given at the end.

#### 3.2.3.1 $P_{surf}$ Using the POWER Dump Files.

It is not clear whether Fichtl cites an instantaneous power or a time-averaged power when presenting his results. Since it is impossible to directly measure the amount of power deposited in the dielectric in the course of an ICEPIC simulation, Fichtl measures the input power, the power transmitted through the dielectric on the right hand side of the system and the power reflected back through the left hand side of the system. Then, he uses the following formula to calculate the power deposited on the surface of the dielectric window under consideration:

$$P_{surf} = P_{input} - P_{reflected} - P_{transmitted} \quad (30)$$

Using this method, Fichtl produces a plot of the fraction of power deposited on the dielectric window (shown in Figure 17). In a similar fashion, the POWER dumps were used to obtain the relevant values for the simulations performed through the course of this research.

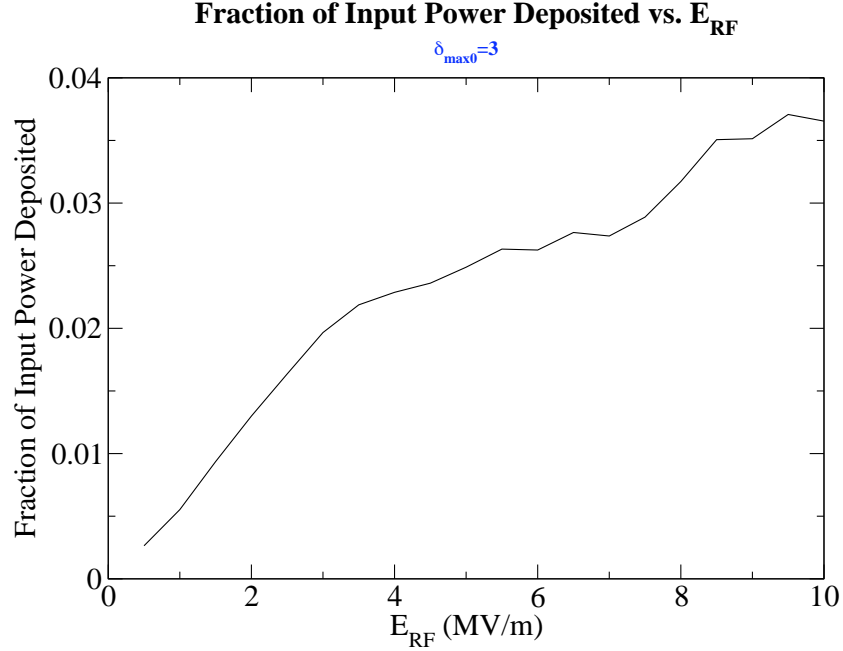


Figure 17. Fraction of input power deposited on the dielectric window as calculated by Fichtl [7]

The theoretical input power can be found by using the Poynting vector:

$$S = \frac{1}{2}c\epsilon_0 E_{RF0}^2$$

Which can then be multiplied by the emitting area to give the average input power:

$$P_{in,thy} = Sx_{sys}y_{sys} = \frac{1}{2}c\epsilon_0 E_{RF0}^2 x_{sys}y_{sys} \quad (31)$$

This theoretical input power is used as a benchmark to ensure the calculations in the following sections are reasonable.

### 3.2.3.2 $P_{surf}$ Using PART Dump Files.

While Fichtl's method is a perfectly acceptable one, independent validation of results is always desirable for consistency and additional insight. ICEPIC affords a

method to dump the properties of every particle that is collected at any boundary in the system. Due to the relatively long length of the system in the  $z$ -direction and the symmetry in the  $x$ -direction, very few particles are collected by the dielectric on the left side of the system. Therefore, it can be assumed that every particle that would be reported by this dump is collected at the boundary of the dielectric under study. The velocity information from this PART dump file can be used in conjunction with the macroparticle weighting information to calculate the energy and, in effect, the power deposited to the surface over a given dump interval. The particle dump files are written every certain number of time steps, defined by the `dump_int` variable in the input file. In our case, `dump_int` was set to dump every 1/50th of a period, where a period is 17,141 time steps and a time step ( $dt$ ) is  $\sim 2.38 \times 10^{-14}$  s. The dump file format includes the position vectors  $(x, y, z)$  as well as the velocity vectors  $(v_x, v_y, v_z)$  for each of the collected particles. All that remains to be found at this point is the macroparticle weighting, which is also included in the dump file, since the charge for each macroparticle is also included in the dump file. Therefore, the mass of the macroparticle,  $M_{macro}$ , is found by using the macroparticle to electron ratio ( $q_{macro}/q_{electron}$ ):

$$M_{macro} = \frac{q_{macro}}{q_{electron}} m_{electron}$$

Then, the Energy can be calculated for each ( $i$ th) particle during a given dump interval, using:

$$\mathcal{E}_{macro,i} = \frac{1}{2} M_{macro} v_{total,i}^2$$

where,

$$v_{total,i}^2 = v_{x,i}^2 + v_{y,i}^2 + v_{z,i}^2$$

Since each dump interval corresponds to a fixed time period, the individual power

can then be calculated from:

$$P_{macro,i} = \frac{\mathcal{E}_{macro,i}}{dt} = \frac{\frac{1}{2}Wm_e v_{total,i}^2}{dt} \quad \text{where} \quad W = \frac{q_{macro}}{q_{electron}}$$

Then the total power is summed for all the particles (over  $i$ ) in the dump file, leading to a total power deposited on the surface by the macroparticles ( $P_{total,macro}$ ). Since these quantities have already been adjusted to account for the macroparticle weighting, this is the total power deposited on the surface of the dielectric. Thus, calculating the power deposited on the surface of the dielectric is a simple matter of using the velocities of the impinging electrons and the macroparticle weighting to calculate the energy per time step deposited on the surface of the dielectric. Since the impinging electrons are the only source of power deposited on the surface, this appears to be the most accurate and straightforward method of determining the power deposited on the surface of the dielectric.

### 3.2.3.3 Theoretical Value of $P_{surf}$ Using Valfells' Theory.

A third possible method of calculating the power deposited on the surface of the dielectric provides a theoretical estimate. This method can then be compared with the previous results for further clarity and insight. Upon reexamination of Equations 19 and 21, it is evident that the only unknown parameter is  $n_0$ . However, it is possible to estimate an average total number of particles from the ICEPIC simulations and solve Equation 16 numerically, to obtain a value of  $n_0$  (the average number density at  $x = 0$ ). Care must be taken to convert from macroparticles to real particles using the macroparticle to electron ratio when performing this calculation. In order to calculate  $n_0$ , Equation 16 is integrated over all  $x$  (or, in the case of our geometry,  $z$ ) and set equal to the average number of real particles determined from the ICEPIC

simulation, as is shown in Equation 32:

$$\frac{n_{total}}{dxdy} = \int_0^{z_{max}} n(z) dz = n_0 \int_0^{z_{max}} \left(1 + \frac{\omega_p}{v_t}\right)^{-2} dz \quad (32)$$

where  $n_{total}$  has been divided by  $dxdy$  in order to simplify what is really a triple integral lurking in Equation 16 (since the equation describes a number density). Then, Equation 32 can be integrated numerically and  $n_0$  obtained through a back solve process. This is necessary since  $\omega_p$  also depends on  $n_0$ . Once  $n_0$  is obtained, it may be used, along with the other parameters (which are known and precisely define the particular simulation) to calculate the approximate theoretical power deposition on the dielectric surface. As this is a mathematically intensive operation which is to be performed over many iterations, **Mathematica**<sup>®</sup> software was used as an aid. The full notebook is contained in Appendix E. Due to the approximate manner in which the total number of macroparticles in the system is found, the result is relied upon as a pure approximation.

### 3.2.3.4 Comparison of Results for Power Deposition on the Dielectric Surface.

This section presents a comprehensive comparison of the three previously discussed methods and Fichtl's results. Since the electron density varies temporally, it is clear that the power deposited on the surface also varies in time. Therefore, any values shown in the table below which are obtained from an ICEPIC simulation are time-averaged over a few periods in the early evolution of multipactor. The values for Fichtl were obtained by direct inspection of Figure 17. Each column header denotes the specific method by which the  $P_{surf}$  (as a percentage of the input power) was calculated. The final column is the  $n_0$  value in real particles/m<sup>3</sup>.

**Table 2. Comparison of Fichtl’s values for power deposited on a dielectric with the values found using the methods detailed in this section.**

$E_{RF}$ (MV/m)	Input Power (W)	$P_{surf}$		
		Fichtl	POWER dump files	PART dump files
1.5	$9.14 \times 10^2$	0.85%	1.78%	2.18%
3.0	$3.66 \times 10^3$	1.90%	6.06%	7.27%
5.5	$1.23 \times 10^4$	2.5%	24.95%	29.09%
7.0	$1.99 \times 10^4$	2.65%	49.27%	53.21%

$E_{RF}$ (MV/m)	$P_{surf}$	
	Valfells’ theory	$n_0$ (real particles/m <sup>3</sup> )
1.5	1.50%	$4.80 \times 10^{19}$
3.0	1.92%	$5.29 \times 10^{20}$
5.5	2.64%	$5.28 \times 10^{22}$
7.0	2.83%	$2.12 \times 10^{23}$

### 3.3 Mitigation Methods

#### 3.3.1 Thin Coatings of Low-SEY Materials.

Adjusting the secondary emission properties is a fairly simple task in an ICEPIC input file. While the secondary emission properties of a material are difficult to measure, Montero, et al. [13] provide a good recent reference for the properties of thin TiN films. Some of the parameters remain unknown and must be estimated based on an educated guess. For the purposes of this research, the following parameters were considered in simulating a system in which the dielectric window is coated with a low-SEY material, such as TiN:O:

The results of these simulations will be discussed in Chapter IV.

#### 3.3.2 Geometrical Modification of the Waveguide/Window Interface.

Valfells, et al. [15] investigate the effects of an obliquely incident RF field, as shown in Figure 10. Following their theoretical development, MATLAB<sup>®</sup> code was

**Table 3. Parameters used to simulate a thinly coated dielectric surface.**

$\delta_{max0}$	1.1
$\mathcal{E}_{max0}$	300 eV
$k_s$	1
$T$	2.1 eV

developed to numerically calculate the susceptibility curve for theoretical system for a given angle of incidence,  $\psi$ . The methodology is described below, while the full code is contained in Appendix C. Also, a method to simulate oblique incidence using ICEPIC without modifying the geometry was developed and is described in section 3.3.2.2.

### 3.3.2.1 Theoretical Model - Matlab<sup>®</sup> for the NSC Case.

The initialization parameters for the code are the angle of incidence ( $\psi$ ), vectors of values for  $E_{DC}$  and  $E_{RF}$  and the secondary emission parameters ( $f$ ,  $\mathcal{E}_{max0}$ ,  $\delta_{max0}$ ,  $k_s$ ,  $\zeta$ ,  $\phi$  and  $v_0$ ). The  $E_{DC}$  and  $E_{RF}$  vectors can be modified to adjust the "resolution" of the caclulations. Note that  $E_{DC}$  and  $E_{RF}$  are scaled to the dimensionless normalization constants used by Valfells, et al. [15]. This is described in detail in the header notes of the MATLAB<sup>®</sup>file contained in Appendix C, but is repeated here for convenience:

$$\begin{aligned}
 t &= t_{real}\omega \\
 v &= v_{real}\frac{1}{\sqrt{\mathcal{E}_{max}/m}} \\
 \mathcal{E} &= \mathcal{E}_{real}\frac{q}{m\omega\sqrt{\mathcal{E}_{max}/m}} \\
 x &= x_{real}\frac{\omega}{\sqrt{\mathcal{E}_{max}/m}}
 \end{aligned}$$

where  $t$  represents time,  $\omega$  is the angular frequency,  $v$  is the velocity,  $\mathcal{E}_{max}$  is  $\mathcal{E}_{max0}$  in units of Joules,  $m$  is the mass of an electron and  $x$  represents the direction normal

to the surface. First, an angle of incidence is selected. Then, within an "inner loop", a value is selected for  $E_{DC}$ . This "inner loop" is eventually run over all the values contained in the  $E_{DC}$  vector. Then, in another loop outside of that one, the value for  $E_{RF}$  is varied in the same manner. For each combination of  $E_{DC}$  and  $E_{RF}$ , the hop time is estimated, using the two dimensional equations of motion similar to those given in Equation 2.2, except that they are modified to account for the angle of incidence. This is done for particles emitted at 50 different phases within the period of  $E_{RF}$ , in order to account for random phase emission of particles, and averaged over those phases. In the following development,  $a_x$  is the  $x$ -directed acceleration,  $a_y$  is the  $y$ -directed acceleration,  $\phi$  is the injection angle of the particles,  $\theta$  is the phase of the electric field at the time of emission and  $\psi$  is the oblique angle of incidence. Using these definitions, the equations of motion are:

$$\begin{aligned} -a_x &= E_x = E_{DC} + E_{RF} \sin(t + \theta) \sin(\psi) \\ -a_y &= E_y = E_{RF} \sin(t + \theta) \cos(\psi) \end{aligned}$$

Then, using the initial conditions, where  $v_{x0}$  and  $v_{y0}$  are the  $x$ - and  $y$ -directed components of the emission velocity:

$$\begin{aligned} v_x(0) &= v_{x0} \sin(\phi) & \text{and} & & x(0) &= 0 \\ v_y(0) &= v_{x0} \cos(\phi) & \text{and} & & y(0) &= 0 \end{aligned}$$

the complete set of equations can be solved, yielding:

$$v_x = -E_{DC} t + v_{x0} \sin(\phi) + E_{RF} (-1 + \cos(t)) \cos(\theta) \sin(\psi) - E_{RF} \sin(t) \sin(\theta) \sin(\psi) \quad (33)$$

$$v_y = v_{x0} \cos(\phi) + E_{RF} (-\cos(\theta) + \cos(t + \theta)) \cos(\psi) \quad (34)$$

$$x = -\frac{E_{DC} t^2}{2} + tv_{x0} \sin(\phi) + E_{RF} \cos(\theta) (\sin(t) - t) \sin(\psi) - E_{RF} \sin(\theta) \sin(\psi) + E_{RF} \cos(t) \sin(\theta) \sin(\psi) \quad (35)$$

$$y = tv_{x0} \cos(\phi) + E_{RF} \cos(\psi) (-t \cos(\theta) - \sin(\theta) \sin(t + \theta)) \quad (36)$$

Since, at this point in all the loops, all quantities are known, except for  $t$ , the hoptime can be found by setting Equation 35 equal to zero (defined as the two points at which the particle is at the dielectric surface) and solving for the corresponding roots. In this code, the hoptime is obtained numerically, using the `fzero()` function in MATLAB<sup>®</sup>. Once it is obtained, the hoptime is used to calculate  $\mathcal{E}_i$ ,  $\zeta$ ,  $\delta$ ,  $\mathcal{E}_1$ ,  $\mathcal{E}_2$  and  $\mathcal{E}_{max}$  from the equations of motion. The secondary emission coefficient ( $\delta$ ) is averaged over the 50 emission phases for each pair of  $E_{RF}$  and  $E_{DC}$ , yielding  $\delta_{avg}$ . If the value for  $\delta_{avg}$  is less than one, it is plotted as a blue circle and if it is greater than one, it is plotted as a red plus. The rest of code is then looped for many different angles of obliqueness. The results of these calculations are given in Chapter IV.

### 3.3.2.2 ICEPIC Model.

To date, no ICEPIC simulations of obliquely incident fields have been performed to verify the narrowing of the multipactor boundary curves. Because of the limitations of the commands that must be used to create shapes in ICEPIC input files, creating a new geometry for these ICEPIC simulations would be incredibly complex and time-consuming. Therefore, the time variable capabilities contained within ICEPIC were applied to the  $E_{DC}$  field to simulate the interaction of the  $E_{RF}$  field with the  $E_{DC}$  field, in the NSC case. The theory behind this simplification is relatively straightforward. According to Figure 10 the  $E_{RF}$  field is described by:

$$E_{RF} = E_{RF0} \sin(\omega t + \theta)$$

However, in the case of an obliquely incident RF field,  $E_{RF}$  takes the form of:

$$E_{RF} = E_{RF0} \sin(\omega t + \theta) \sin(\psi)$$

As electrons leave the surface,  $E_{DC}$  evolves as a "constant" field. Therefore, the total field in the  $z$ -direction is given by (also assuming the simulation starts when  $\theta = 0$ ):

$$E_{z,tot} = E_{DC} + E_{RF0} \sin(\omega t) \sin(\psi)$$

This leads to a time-varying  $E_{DC}$  field, which is predicted by Valfells, et al. [15]. This time varying  $E_{DC}$  will naturally lead to a change in the susceptibility of the system to multipactor. It is worth noting, though, that previous research did not consider the time-varying aspect of multipactor evolution, but dealt purely in averages. In our simulations, the time-varying aspect is unavoidable and so the results should be compared with caution. A sample input file is given in Appendix D, where the time variable parameters  $C_0$  and  $C_1$  are used to create the time varying  $E_{DC}$  field. According to the ICEPIC manual, the time variables can be used to create a field described by:

$$E_{DC,\psi} = C_0 + C_1 \sin(\omega t + \theta) + \dots$$

where:

$$C_0 = 1 \quad \text{and} \quad C_1 = (E_{RF0}/ - E_{DC}) \sin(\psi)$$

Figure 18 compares the theoretical output with actual output from a corresponding ICEPIC simulation. The plot in the theoretical case has been shifted to the right to account for the propagation delay in the simulation. This is due to the fact that the wave is launched from the left hand dielectric, propagates for a finite amount of time and is measured at the right hand dielectric surface. Also, in the plots of the fields

from the simulation, a "ramp up" time is noticeable for both the  $E_{RF}$  and  $E_{DC}$  fields to move to the expected values, which is a function of the time variable configuration in ICEPIC and unavoidable.

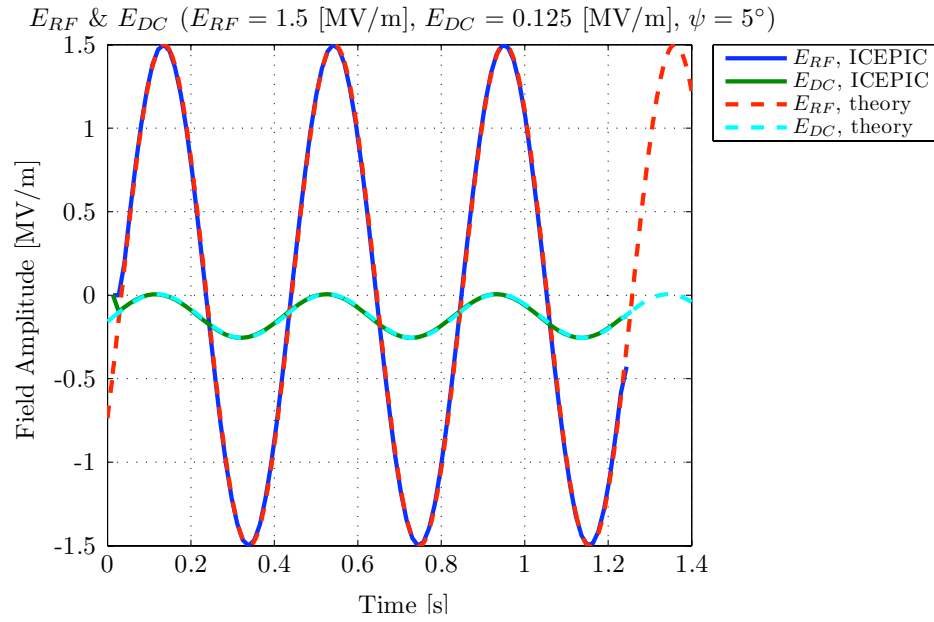


**Figure 18.** Comparison of the theoretical and ICEPIC  $E_{DC}$  and  $E_{RF}$  fields in the oblique case. The theoretical case has been run out to longer times than

## IV. Analysis of Results

This chapter looks at the results of the results from the calculations and simulations described in Chapters II - III and presents some analysis regarding these results, relating them to the comprehensive purpose of multipactor mitigation in HPM systems. The destructive mechanism of multipactor is twofold. First and foremost, the continual bombardment of the dielectric surface by high energy electrons results in the deposition of a percentage of the input power on the surface of the dielectric. This power deposition eventually results in damage to the dielectric surface, eventually causing system failure. This limits the input power of an HPM system. Also of interest is how the field strength of this limit compares with the breakdown field strength of air, which is a fixed threshold. Secondly, the high density of electrons reflects a portion of the  $E_{RF}$  field being reflected back towards the source in a real HPM system. Eventually, this can result in damage to or failure of the source. Both of these mechanisms are discussed below, followed by the effect of the proposed mitigation strategies.

### 4.1 Multipactor Power

The power absorbed by the electrons of a multipactoring system can be viewed in many different ways. As was previously stated, the power deposition on the surface of the dielectric is of primary interest. Also of concern is the power reflected back towards the source by the evolving electron density, which can result in damage to the HPM source. Also, whether or not multipactor supercedes the limit imposed by air breakdown is considered in this section.

### 4.1.1 Power Deposition.

As is evident from Table 2, the `PART` dump and `POWER` dump methods of determining power deposited on the surface of the dielectric correlated well, but produced drastically different results than the method using Valfells' theoretical method and Fichtl's results. This remains an unreconciled discrepancy. The two different dump files used from ICEPIC simulations are independent of one another and are well tested. Also, the input power from the dump files match up almost exactly with the theoretical input power, as calculated in Equation 31. Since the `PART` dump method uses basic physics to calculate the kinetic energy and power associated with a particle impacting the dielectric surface over a short time, this seems to be the simplest and most trustworthy method. However, it is possible that ICEPIC contains a code bug that incorrectly reports values to either both of these dump files, or a power sink exists that has been overlooked. Fichtl [7], considers later times, but this would represent an increase in the amount of power deposited on the dielectric surface, since the electron density would also be higher. It is unclear what these results signify and how they should be interpreted. Further study is recommended to correlate these results to the literature.

### 4.1.2 Reflected Power.

In the course of performing ICEPIC simulations, an interesting phenomenon came to light. For many simulations, at lower values of  $E_{RF}$ , the amount of reflected power was on the order of tenths of a percent of the input power. However, as both the particle weighting and value of  $E_{RF}$  were increased, and the simulations were allowed to run out to longer times, the reflected power was seen to greatly increase. While increasing the particle weight was geared to decrease the simulation time, it had the unintended result of producing very high real electron densities at these later times.

In fact, at electron densities on the order of  $5 \times 10^{19}$  electrons/m<sup>3</sup>, a near complete reflection of input power occurred. This is not accounted for in any of the current theories. It is possible that this phenomenon could account for the "knee" Fichtl notes in his power deposition analysis. The power deposited on the surface should rise proportional to the  $E_{RF}$ , however, when an increasingly larger amount of power is reflected, the power deposited on the surface would decrease accordingly. Obviously, reflected power is of great concern to preserving expensive and sensitive HPM sources.

### 4.1.3 Multipactor Power Limit versus Air Breakdown Limit.

Ambient air breakdown is a fixed limit, one that truly restricts every HPM system. In the case where SC is considered, the susceptibility curve is no longer interpreted as a metric of whether or not multipactor occurs, but it describes the system trajectory in susceptibility space as it moves through regions of electron growth and decay. However, there are still some values of  $E_{RF}$  for which multipactor does not occur, because the RF field does not impart enough energy to the electrons to facilitate multipactor growth. Where this boundary falls in relation to the fixed limit of ambient air breakdown holds drastic implications for the future of higher powered systems. A series of ICEPIC simulations was performed to find this lower boundary and the value of  $E_{RF}$  at which a system no longer sustains multipactor growth is approximately 0.25 MV/m. The field breakdown strength of ambient air at sea level, for a reasonably assumed emitting area of 1 m<sup>2</sup> is given to be 2.745 MV/m [2]. In the context of the "bowtie" plots (see Figure 16), the behavior correlates well with our current understanding of multipactor. As the overall amplitude of  $E_{RF}$  decreases, the total number of particles in the system decreases as well. Therefore, both the height and width of the "bowtie" decrease, to the point where the "bowtie" no longer makes excursions into the region of multipactor growth and all the particles in the system

are lost to the dielectric surface. Therefore, since the multipactor limit is lower than the ambient breakdown limit, it is evident that this is the reason why multipactor remains a serious concern in the design and implementation of HPM systems. The upper limit was found to be greater than  $1 \times 10^9$  V/m, which is well above the capabilities of modern systems, so the upper limit is not considered.

## 4.2 Mitigation Techniques

### 4.2.1 Geometric Modification of the Waveguide/Window Interface.

Using the code described in Section 3.3.2.1, susceptibility curves for a certain system were generated for the NSC case. These curves are shown in Figure 19. From these curves, it is found for smaller angles of incidence,  $\psi \sim 5 - 10^\circ$ , the susceptibility region actually increases. However, for angles of incidence greater than or equal to  $10^\circ$ , the susceptibility region begins to dissipate and then contracts rapidly. At angles greater than  $20^\circ$ , the system appears to be no longer susceptible to multipactor at all. It is not clear from this research whether or not the susceptibility actually disappears or if this is numerical artifact. Regardless, the diminished region of susceptibility is promising and confirms the theory.

With regards to the ICEPIC simulations, the results are not as conclusive as with the MATLAB<sup>®</sup> calculations. The results of the simulations are compared with the MATLAB<sup>®</sup> results in Figure 20. From these simulations, it is clear that the results correlate well with the theory and, in fact, show the lower boundary moving up. It is unclear what the SC case might produce in ICEPIC simulations. One can imagine, though, from looking at Figure 16, that since the susceptibility range is significantly reduced, the system trajectory may spend less time in the range which represents multipactor growth and, therefore, reach a periodic steady state at a lower average electron density. Therefore, one might anticipate that less power would be deposited

on the dielectric surface and less power would be reflected towards the source. This, in turn, would allow systems to operate at higher powers before reaching the point where enough power is deposited on the surface to cause failure of the dielectric.

#### **4.2.2 Thin Coatings of Low-SEY Materials.**

Reducing the secondary emission coefficient of the dielectric surfaces has the primary effect of reducing the electron density in the system, which gives a twofold advantage: a reduction in the power deposited on the surface of the dielectric and a reduction in the electron density of the system which equals less power reflected towards the source. Figure 21 compares the power deposited on the surface of the dielectric for the same four cases run in Table 2. It is evident from Figure 21 that the power deposited on the surface of a dielectric is drastically reduced for a system coated in a film like Ti:N.

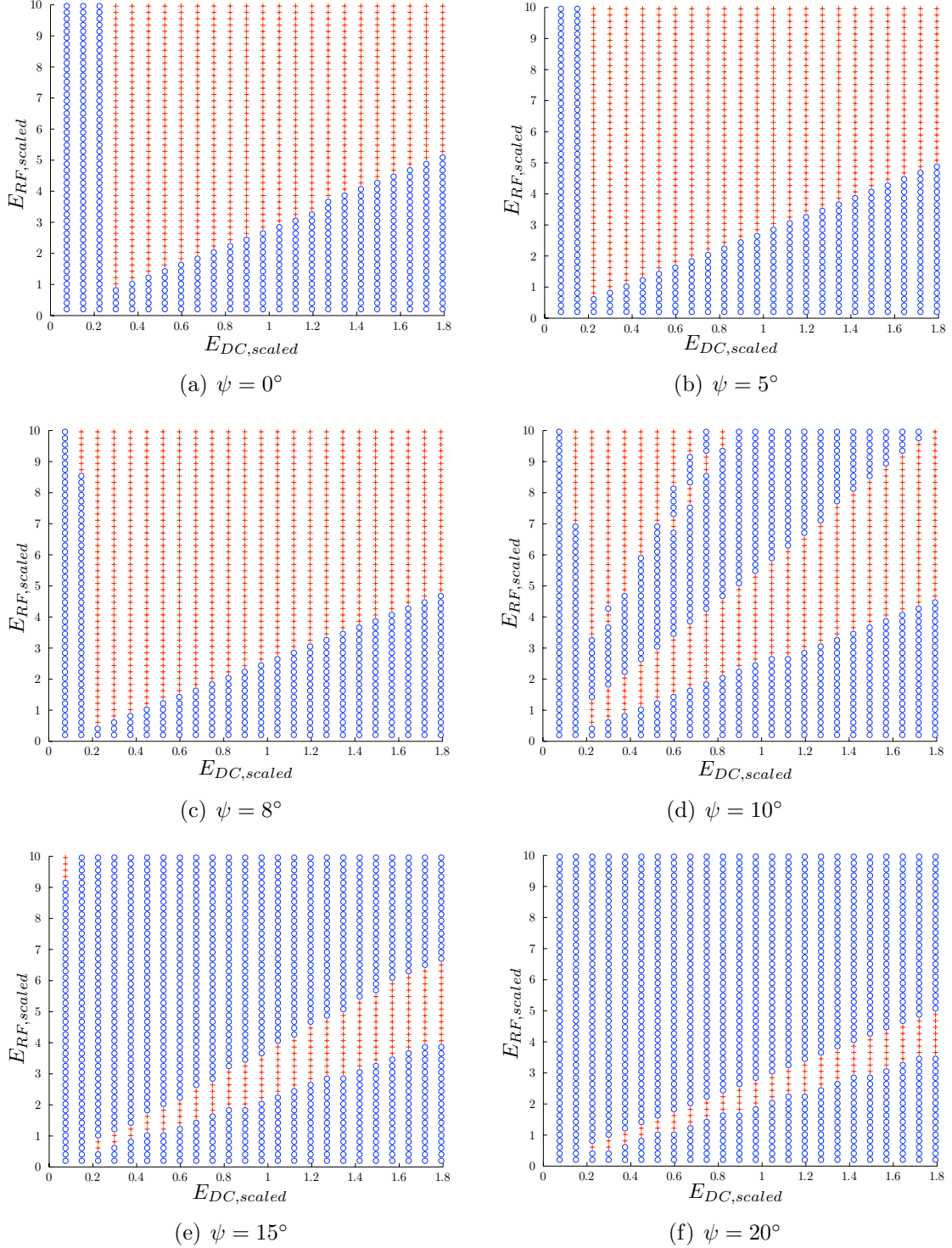
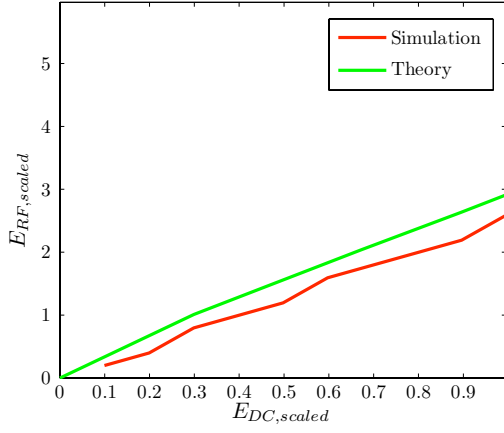
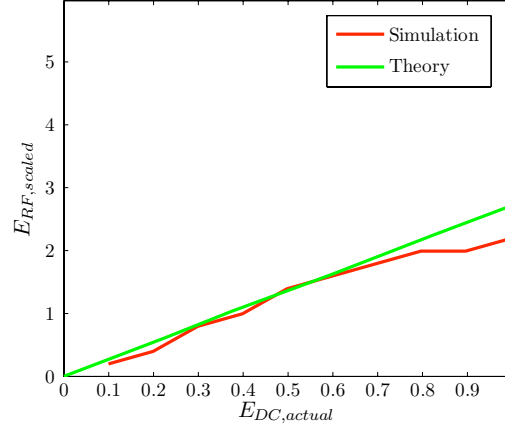


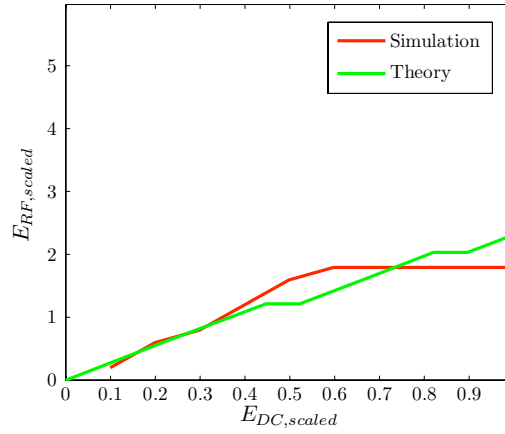
Figure 19. Susceptibility curves generated from Matlab<sup>®</sup>simulations, where  $E_{DC}$  and  $E_{RF}$  are scaled as  $[\text{MV/m}] \times (f/1\text{GHz})^{-1} (\mathcal{E}_{max0}/400\text{eV})^{-1/2}$ . In this system,  $\delta_{max0} = 3$ . Plus signs (+) represent points at which multipactor occurs and circles (o) represent areas where multipactor does not occur.



(a)  $\psi = 0^\circ$



(b)  $\psi = 10^\circ$



(c)  $\psi = 15^\circ$

**Figure 20.** Susceptibility curves generated from ICEPIC simulations, where  $E_{DC}$  and  $E_{RF}$  are scaled as  $[\text{MV}/\text{m}] \times (f/1\text{GHz})^{-1} (\mathcal{E}_{max0}/400\text{eV})^{-1/2}$ . In this case, only the lower boundary is shown.

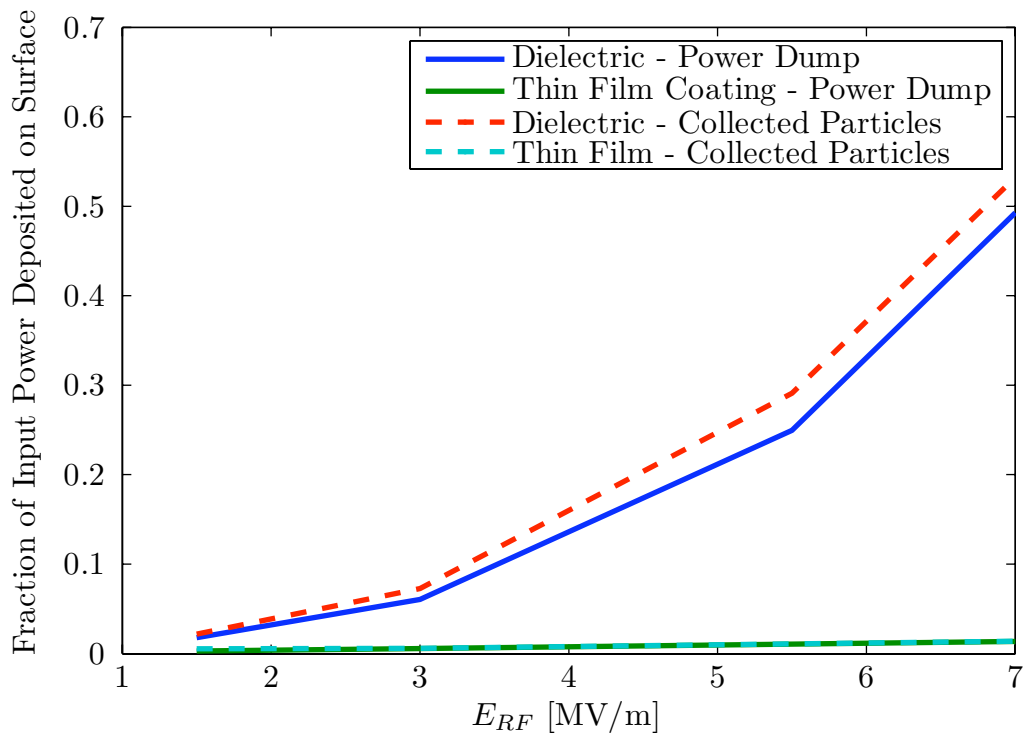


Figure 21. Comparison of the power deposition metrics for the bare dielectric and the dielectric covered by a thin coating of a low-SEY material.

## V. Conclusions and Future Work

### 5.1 Conclusions

Chapter II presented the basic theory of multipactor and offered a short summary of the known theory relating to this phenomenon. Secondary Electron Emission (SEE) in materials is the underlying phenomenon leading to a net gain in electrons, or a SEY greater than one and an eventual electron avalanche in HPM systems. Secondary emission is well described by Vaughan in [17] and is dependent on a few parameters of the impacted material, as well as the energy of the impacting electrons. Both the NSC and SC cases were discussed, along with the different interpretations of each case. In the NSC case, "universal" multipactor boundaries may be constructed, normalized to  $E_{max0}$  and  $f$ , so that multipactoring regimes may be predicted for many systems. For the SC case, the electron density and, accordingly,  $E_{DC}$  varies both spatially and temporally, so the theory differs and the susceptibility curves must be also be interpreted according to the temporal variation. In light of this discovery, the term " $E_{DC}$ " is misleading, since, in reality, the restoring field is not constant. However, in order to be consistent with the literature and current jargon, the term  $E_{DC}$  is still used. So-called "bowtie" diagrams can be created from the relationships between  $E_{RF}$  and  $E_{DC}$  and the guidelines from the NSC case estimate when the secondary emission coefficient is greater than one and when it is less than one. An overview of general PIC code theory and input parameters served as the foundation for understanding ICEPIC results and how secondary emission effects are included in ICEPIC simulations. With regard to mitigation methods, two methods were discussed in this paper - thin coatings of low-SEY materials and RF field oblique incidence. The theory behind each was discussed.

In Chapter III, the rationale behind the selected input parameters was discussed,

along with a detailed description of important variables in ICEPIC. Then, current simulations were compared with those presented in the literature. ICEPIC simulations confirmed the results of both Verboncoeur [9] and Fichtl [7], while updates to the code resulted in small changes in the universal susceptibility curves. Current ICEPIC simulations show that, in some cases (values of  $E_{RF}$  less than 3.0 MV/m), at relatively short times ( $\sim 5$  periods), the particle density reaches a periodic steady state. In some cases, though, the particle density continues to rise slowly throughout the simulation and may, at longer times, reach a similar steady state. For the purposes of this paper, the early evolution of multipactor is studied, where values for power and fields are reported between five and eight periods. While this may not, in every case, represent a true "steady state," it is taken to accurately represent a snapshot in time of the order of magnitude of multipactor and can be extended to longer times. Power deposition on the surface is perhaps the most destructive effect of multipactor, resulting in failure of the dielectric window. Therefore, a large amount of time was spent understanding and analyzing power deposition. Three different methods were used to estimate the power deposited on the surface. Two of the methods, independent dumps from the ICEPIC simulations, confirmed each other, while the third, implementing the space charge theory from [16] correlated well with Fichtl's results in [7]. The reason for the large disparity between the two different results remains unreconciled. Since Fichtl's input files were the basis for the simulations presented in this paper and all known, realistic power sinks were accounted for, no determination can be made yet as to the source of this disparity. Additionally, the ICEPIC models behind the two mitigation methods were presented, and the computational theory behind development of susceptibility curves in MATLAB explained.

It has been demonstrated that multipactor growth occurs very quickly in a system, usually within a few nanoseconds. Considering that a pulse in an HPM system

may be on the order of 100 ns, it is clear that a large amount of power may be deposited on the surface of the dielectric in a very few pulses. Analysis of the results of power deposition metrics and simulations for the mitigation methods was presented in Chapter IV. It was found that the electron density is important not only because of the power deposited on the surface of the dielectric, but because higher densities reflect large amounts of power back towards the source and may result in damage to the HPM source.

For the SC case, lower and upper boundaries were found - outside of which multipactor no longer occurs within a system. The breakdown field strength of ambient air is between these two values, emphasizing the need to consider multipactor evolution and, most certainly, mitigation methods, when designing an HPM system.

Also presented in Chapter IV is an analysis of the effects of RF obliqueness and on the susceptibility curves. The curves are significantly narrowed for angles of obliqueness greater than  $10^\circ$ . Since it is primarily the upper boundary that shifts when considering an obliquely incident RF field and it is the lower boundary that is primarily associated with electron saturation, the goal would be to create a system in which the angle of obliqueness is greater than  $20^\circ$ , so that the susceptibility to multipactor would be very small. It was also found that, due to a narrowing of the susceptibility region, in a carefully designed system, less power may be deposited on the dielectric. Therefore, systems with higher input powers may be developed.

In general, it is found that both mitigation methods that were explored in this paper result in a dampening, and, for some systems, total elimination, of electron multipactor growth and a decrease in the amount of power deposited on the surface of the dielectric. Therefore, a combination of these two methods deserves further study through simulation and consideration when designing current and future HPM systems.

## 5.2 Future Work

Many aspects of the work presented in this paper require further work in order to justify their inclusion in modern HPM systems. Some of these aspects are natural extensions of the research described in this paper, while others are required to further solidify the correlation between simulation and theory. Suggestions for future work are made with the goal of obtaining a more complete and physically accurate model for simulating the multipactor phenomenon and the possible mitigation techniques discussed in this paper (as well as future techniques).

The simulations that were run during the course of this research were very specialized; they considered only the multipactor effect inside the system for generic, widely-accepted and utilized parameters. However, it is not known how the parameters of current simulations compare with more realistic parameters (i.e. size, emissivity) of real dielectric windows. One possible area for future work is to update these parameters and analyze the effects of multipactor in a more realistic sense.

While some simulations of a system in which the dielectric was coated with a thin, low-SEY material were conducted, a few assumptions were made in running these simulations. Each of these assumptions should be studied and tested, so as to be proven or discarded in future simulations. Most importantly, it was assumed that the SEY coefficient of the dielectric surface is reduced to that of the thin film covering. However, it is unclear if this is actually the case. It is possible that some electrons strike the surface and penetrate to the original dielectric. Obviously, this is highly dependent on the thickness of the thin film. Therefore, the average secondary coefficient may be reduced by some amount less than was assumed in this paper. A model could be developed which includes the physics of multiple layers of materials with different SEY coefficients. This model could then be used to study the necessary thickness of the coating of a low-SEY material.

This paper describes a few simulations that were run to emulate an obliquely incident RF field for the NSC case by using the time variables inherent in ICEPIC. This is useful in determining the multipactor boundaries as presented by Kishek, et al. [11]. However, the power deposition on the surface cannot be studied accurately in this case, since the space charge effects are ignored. Therefore, it would be useful to run these simulations in the SC case. This would require altering the geometry of the system to include a window that includes an RF window that is physically oblique to the incoming RF field. This would be a complex undertaking in ICEPIC, due to many of the unknown factors, two of which are: actually creating the geometry in ICEPIC and understanding how the PML boundaries handle this type of geometry, since it now appears asymmetric to the PML. Implementing a truly oblique geometry in ICEPIC would allow simulation and analysis of many types of multipactor-inhibiting geometries, to more accurately determine the effectiveness of this mitigation strategy.

According to [3], outgassing effects at the surface of the dielectric produce an as yet unknown quantitative variation in the SEY of the system. Since impacting electrons will cause desorption of gas at the dielectric surface, at certain levels of  $E_{RF}$ , a layer of gas may form above the surface of the dielectric (a process in itself not well understood) and potentially form a plasma, resulting in near total reflection of the incident power. The effect of this gas layer on electron multipactor in the system is not well studied and deserves further attention.

# Appendix A. Sample ICEPIC Input File for Non-Space Charge Case

This input file is for the non-space charge case.

```
1 [Defaults]
ENERGY=1.5e6 ; these parameters can be varied for surveys
EDC=0.125e6

; this is fichtl's original file case and is meant to recreate his...
thesis work.
6 ; it has been updated to work with current versions of ICEPIC.

[Variables]
c0=299792458.0
pi=3.141592653589793
11 eps0=8.85418781762E-12
me=9.1093897E-31
qe=1.60217738E-19
test=1
fc=2.45E9
16 lamda0=c0/fc
ez=EDC
energy=ENERGY
dz=lamda0/3000 ; determines the z-resolution of the system
PMLdepth=int((.025*lamda0)/dz+.5)
21 Nx=50
Nz=300
xmin=0
xmax=Nx*dz
zmin=0
26 zmax=Nz*dz
dt=0.99*dz/(c0*sqrt(2))
period=int(1/fc/dt)
maxstep=15*period
hoptime=(2*me/qe/ez)*sqrt(2*qe*420/me)*0.8509035245 ; this is ...
worst-case
31 hopdist=sqrt(2*qe*420/me)*hoptime
Ndielect=10*dz
print "Hop time=", hoptime ; comments in the *.dat file
print "Hop distance=", hopdist
print "TimeSteps/Hoptime=", hoptime/dt
36 print "Hop distance/dz=", hopdist/dz

[Cartesian]
ig_dir=(0,1,0)
default_e=(0.,0.,-ez)
41 [XGrid1]
range=Uniform(xmin-3*dz,xmax+3*dz,Nx+6) ; accomodates symmetry ...
shortcomings
```

```

[YGrid1]
46 range=Uniform(0,1,1)

[ZGrid1]
range=Uniform(zmin,zmax,Nz)

51 [Symmetry]
;symmetry=(xmin,-1.,zmin-10*dz,xmax,2.,zmax+10*dz)
periodic1=(X,xmin,xmax)
;sym mode=(1.0,0.0,0.0)

56
[Time]
dt=dt
step_max=maxstep
courant_value=.95
61 kill_if_below_parts=5
kill_if_above_parts=2e6

[ShapeN]
; computational domain
66 shape=Box(xmin,xmin,zmin,xmax,xmax,zmax)

[ShapeN]
;Dielectric on RHS of system
shape=Box(xmin,0.0,zmax-4*dz-PMLdepth*dz-Ndielect,xmax,1.0,zmax-4*...
dz-PMLdepth*dz)
71 material=dielectric

[ShapeN]
;Dielectric on LHS of system
shape=Box(xmin,0.0,zmin+4*dz+PMLdepth*dz,xmax,1.0,zmin+PMLdepth*dz...
+Ndielect+4*dz)
76 material=dielectric

[MaterialN]
name=dielectric
epsilon=1.001
81
[ParticlesN]
;Secondary emitter on dielectric on RHS of system
shape=Box(xmin-dz,0.0,zmax-4.25*dz-PMLdepth*dz-Ndielect,xmax,1.0,...
zmax-3.75*dz-PMLdepth*dz-Ndielect)
method=SECONDARY
86 sec_coefficient=3
sec_energy=2.1
sec_threshold=1
sec_refl=0.03
sec_scatt=0.07
91 sec_energy_max_yield=420
sec_ks=1

```

```

q=-qe
mass=me
dir=2
96 [ParticlesN]
;Particle emitter on dielectric on RHS of system
shape=Box(xmin-dz,0.0,zmax-4.25*dz-PMLdepth*dz-Ndielect,xmax,1.0,...
      zmax-3.75*dz-PMLdepth*dz-Ndielect)
method=BEAM
101 temp=2.1/test
energy=0.0/test
random=1
q=-qe/test
mass=me/test
106 current=1000/test
inject_interval=100
flattop=.5/fc
amp2=0
tstop=.5/fc
111 smooth=1
dir=2

[PlanewaveN]
;Generates Planewave from xmin to xmax across system
116 shape=Box(xmin-2*dz,0.0,zmin+PMLdepth*dz+2*dz,xmax+2*dz,1.0,zmax-...
      PMLdepth*dz-2*dz)
theta=180.0
phi=0.0
psi=180.0
frequency=fc
121 origin=(xmin,0.0,zmin+2*dz+dz*PMLdepth)
E0=energy

[Expert]
;cell_mult=12 ;not sure what this parameter is, not in current ...
      ICEPIC version
126 requested_max_num_particles=3e6
self_fields=0 ;this is what turns off the space charge

[BoundN]
;PML on LHS of system
131 method=PML
depth=PMLdepth
R=1.0E-4
taper=0
order=2
136 dir=2
shape=Box(xmin,0,zmin-dz/2,xmax,1.0,zmin+dz/2)

[BoundN]
;PML on RHS of system
141 method=PML

```

```
depth=PMLdepth
R=1.0E-4
taper=0
order=2
146 dir=2
shape=Box(xmin,0,zmax-dz/2,xmax,1.0,zmax+dz/2)

; no dumps for this case, since all we're looking for is mp growth
```

## Appendix B. Sample ICEPIC Input File for Space Charge Case

This input file is for the space charge case.

```
1 [Defaults]
ENERGY=3e6 ; these
EDC=0

; this is fichtl's original file and is meant to recreate his ...
; thesis work in the
6 ; space charge case. it has been updated to work with current ...
; version of
; ICEPIC. put in new field dumps to correspond with the power ...
; dumps and
; shortened the max time of the simulation.
;

11 [Variables]
c0=299792458.0
pi=3.141592653589793
eps0=8.85418781762E-12
me=9.1093897E-31
16 qe=1.60217738E-19
test=1
fc=2.45E9
lamda0=c0/fc
ez=EDC*1e6
21 energy=ENERGY
dz=lamda0/12000 ; finer resolution than the NSC case
PMLdepth=int((.0125*lamda0)/dz+.5)
Nx=3
Nz=200+2*PMLdepth
26 xmin=0
xmax=Nx*dz
zmin=0
zmax=Nz*dz
dt=0.99*dz/(c0*sqrt(2))
31 zbuff=6*dz
period=int(1/fc/dt)
maxstep=8*period
Ndielect=10*dz
numstart=5*period
36 numstop=8*period
DumpInt=period/50
print "PMLdepth=", PMLdepth ; comments in the *.dat file
print "dz=", dz
print "dt=", dt
41 print "Period=", period
print "last step=", maxstep
```

```

[Cartesian]
ig_dir=(0,1,0)
46 default_e=(0.,0.,-ez)

[XGrid1]
range=Uniform(xmin-1.0*dz,xmax+2.0*dz,Nx+3)

51 [YGrid1]
range=Uniform(0,1,1)

[ZGrid1]
range=Uniform(zmin,zmax,Nz)
56

[Symmetry]
;symmetry=(xmin-.25*dz,-1,zmin-10*dz,xmax+.25*dz,2,zmax+10*dz)
;sym mode=(1.0,0.0,0.0)
periodic1=(X,xmin-.25*dz,xmax+.25*dz)
61

[Time]
dt=dt
step_max=maxstep
courant_value=.95
66

[ShapeN]
shape=Box(xmin,xmin,zmin,xmax,1.0,zmax) ; the computational ...
domain

[ShapeN]
71 ;Dielectric on RHS of system
shape=Box(xmin,0.0,zmax-2*zbuff-PMLdepth*dz-Ndielect,xmax,1.0,zmax...
-2*zbuff-PMLdepth*dz)
material=dielectric

[ShapeN]
76 ;Dielectric on LHS of system
shape=Box(xmin,0.0,zmin+2*zbuff+PMLdepth*dz,xmax,1.0,zmin+PMLdepth...
*dz+Ndielect+2*zbuff)
material=dielectric

[MaterialN]
81 name=dielectric
epsilon=1.001

[ParticlesN]
;Secondary emitter on dielectric on RHS of system
86 shape=Box(xmin-dz,0.0,zmax-2*zbuff-0.25*dz-PMLdepth*dz-Ndielect,...
xmax,1.0,zmax-2*zbuff+0.25*dz-PMLdepth*dz-Ndielect)
method=SECONDARY
sec_coefficient=3
sec_energy=2.1/test
sec_threshold=1/test
91 sec_refl=0.03

```

```

sec_scat=0.07
sec_energy_max_yield=420/test
sec_ks=1
q=-qe/test
96 mass=me/test
dir=2

[ParticlesN]
;Particle emitter on dielectric on RHS of system
101 shape=Box(xmin-dz,0.0,zmax-2*zbuff-0.25*dz-PMLdepth*dz-Ndielect,...
      xmax,1.0,zmax-2*zbuff+0.25*dz-PMLdepth*dz-Ndielect)
method=BEAM
temp=2.1/test
;temp=10.0/test
energy=0.0/test
106 random=1
q=-qe/test
mass=me/test
current=2.5/test
;inject interval=10
111 inject=1
flattop=.5/fc
amp2=0
tstop=.5/fc
smooth=1
116 dir=2

[PlanewaveN]
;Generates Planewave from xmin to xmax across system
shape=Box(xmin-2*dz,0.0,zmin+PMLdepth*dz+zbuff,xmax+2*dz,1.0,zmax-...
      PMLdepth*dz-zbuff)
121 theta=180.0
phi=0.0
psi=180.0
frequency=fc
origin=(xmin,0.0,zmin+zbuff+dz*PMLdepth)
126 E0=energy

[Expert]
;cell mult=12 ;not sure what this parameter does - not supported ...
      in current ICEPIC
requested_max_num_particles=3e6
131 self_fields=1 ;ensures space charge is accounted for
[BoundN]
;PML on LHS of system
method=PML
depth=PMLdepth
136 R=1.0E-4
taper=0
order=2
dir=2
shape=Box(xmin,0,zmin-dz/2,xmax,1.0,zmin+dz/2)

```

```

141 [BoundN]
    ;PML on RHS of system
    method=PML
    depth=PMLdepth
146 R=1.0E-4
    taper=0
    order=2
    dir=2
    shape=Box(xmin,0,zmax-dz/2,xmax,1.0,zmax+dz/2)
151
    ;[DumpN]
    ;dump_format=GRID
    ;dump_plane=1
156 ;dump_value=0
    ;nstop=0

    [DumpN]
    dump_format=PART
161 dump_interval=DumpInt
    nstart=numstart
    nstop=numstop
    collected_part=1

166 [DumpN]
    dump_format=FIELD
    dump_plane=1
    dump_value=0
    fieldflags=1-1-1-2-p-1
171 dump_interval=DumpInt
    shape=Box(xmin,xmin,(zmax-PMLdepth*dz-Ndielect-2*zbuff-1*dz)-(zmin...
        +PMLdepth*dz+Ndielect+2*zbuff+1*dz)/2,xmax,1.0,zmax-PMLdepth*dz...
        -Ndielect-2*zbuff-1*dz)
    dump_in_PML=0
    ;;dump_exclude_static=0 ;not supported by current version
    dump_name=fieldSys
176 nstart=numstart
    nstop=numstop

    ;[DumpN]
    ;dump_format=CQUADS
181 ;shape=Box(xmin,xmin,zmin,xmax,1.0,zmax)
    ;nstop=0

    [DumpN]
186 dump_format=FIELD
    dump_plane=1
    dump_value=0
    fieldflags=1-1-1-2-p-1
    dump_interval=DumpInt

```

```

191 dump_name=fieldR
    nstart=numstart
    nstop=numstop
    shape=box(xmin,0,zmin+PMLdepth*dz+(zbuff/2)-0.5*dz,xmax,1.0,zmin+...
        PMLdepth*dz+(zbuff/2)+0.5*dz)

196
    [DumpN]
    dump_format=FIELD
    dump_plane=1
    dump_value=0
201 fieldflags=1-1-1-2-p-1
    dump_interval=DumpInt
    dump_name=fieldB
    nstart=numstart
    nstop=numstop
206 shape=box(xmin,0,zmin+PMLdepth*dz+(3*zbuff/2)-0.5*dz,xmax,1.0,zmin...
        +PMLdepth*dz+(3*zbuff/2)+0.5*dz)

    [DumpN]
    dump_format=FIELD
211 dump_plane=1
    dump_value=0
    fieldflags=1-1-1-2-p-1
    dump_interval=DumpInt
    dump_name=fieldT
216 nstart=numstart
    nstop=numstop
    shape=box(xmin,0,zmax-PMLdepth*dz-(3*zbuff/2)-0.5*dz,xmax,1.0,zmax...
        -PMLdepth*dz-(3*zbuff/2)+0.5*dz)

221
    [DumpN]
    dump_format=POWER
    dump_plane=2
    dump_value=zmax-PMLdepth*dz-(3*zbuff/2)
226 dump_name=powerT
    shape=Box(xmin,xmin,zmin,xmax,1.0,zmax)
    nstart=numstart
    nstop=numstop

231 [DumpN]
    dump_format=POWER
    dump_plane=2
    dump_value=zmin+(3*zbuff/2)+PMLdepth*dz
    dump_name=powerB
236 shape=Box(xmin,xmin,zmin,xmax,1.0,zmax)
    nstart=numstart
    nstop=numstop

```

```

[DumpN]
241 dump_format=POWER
    dump_plane=2
    dump_value=zmin+(zbuff/4)+PMLdepth*dz
    dump_name=powerR
    shape=Box(xmin,xmin,zmin,xmax,1.0,zmax)
246 nstart=numstart
    nstop=numstop

[DumpN]
251 dump_format=POWER
    dump_plane=2
    dump_value=zmax-PMLdepth*dz-2*zbuff-Ndielect-1*dz
    dump_name=powerS
    shape=Box(xmin,xmin,zmin,xmax,1.0,zmax)
    nstart=numstart
256 nstop=numstop

[DumpN]
    dump_format=PROBE
    dump_interval=DumpInt
261 p=((xmax-xmin)/2,0,zmax-2*zbuff-1.25*dz-PMLdepth*dz-Ndielect)

[DumpN]
    dump_format=PROBE
    dump_interval=DumpInt
266 p=((xmax-xmin)/2,0,zmax-2*zbuff-0.25*dz-PMLdepth*dz-Ndielect)

[DumpN]
    dump_format=J_DOT_E
    avg_interval=DumpInt
271 dump_interval=1
    nstart=numstart
    nstop=numstop
    shape=Box(xmin,xmin,(zmax-PMLdepth*dz-Ndielect-2*zbuff-1*dz)-(zmin...
        +PMLdepth*dz+Ndielect+2*zbuff+1*dz)/2,xmax,1.0,zmax-PMLdepth*dz...
        -Ndielect-2*zbuff-1*dz)

276 ;;[DumpN]
    ;; dump_format=DENSITY
    ;; species_num=0
    ;; dump_interval=20
    ;; nstart=14*period
281 ;; nstop=15*period
    ;; dump_local=0
    ;; shape=Box(xmin,xmin,(zmax-PMLdepth*dz-Ndielect-2*zbuff-1*dz)-(...
        zmin+PMLdepth*dz+Ndielect+2*zbuff+1*dz)/2,xmax,1.0,zmax-...
        PMLdepth*dz-Ndielect-2*zbuff-1*dz)

[DumpN]
286 dump_format=RESTART
    dump_interval=1

```

```

force_dump_last=1
nstart=5*period-2
nstop=5*period
291 [Repeat]
Rtype="Dump"
Rindex=0
Rmaxindex=int(((zmax-zmin - 2*PMLdepth*dz)/6.0)/dz)
296 Rstep=1
[BeginRepeating]
dump_format=VOLTAGE
dump_interval=DumpInt
nstart=numstart
301 nstop=numstop
start1=((xmax-xmin)/2.0,0.0,zmax - PMLdepth*dz - Ndielect - 2*...
zbuff)
end1=((xmax-xmin)/2.0,0.0,(zmax - zmin - 2*PMLdepth*dz)*5.0/6.0 +...
PMLdepth*dz - Ndielect - 2*zbuff + Rindex*dz)
num_sample=4*int(((zmax-zmin-2*PMLdepth*dz)/6.0)/dz) - 4*(Rindex...
-1)
[EndRepeat]

```

## Appendix C. Code for Calculation of Theoretical Susceptibility Curves for the Oblique Case in Matlab®

```

% version 2 incorporates printing out the yield based on the
% phase-averaged energy, to compare with the phase-averaged yield
% oblique approach to multipactor susceptibility curves
% dimensionless quantities:
5 %   t = w*t
%   v = v/sqrt(Emax/m)
%   E = q*E/(m*w*sqrt(Emax/m))
%   x = w*x/sqrt(Emax/m)
%
10 % this case finds the phase averaged impact energy, then
% For these parameters:
%
% freq=2.45e+9; % Hz
% w=2*pi*freq;
15 % m=9.8e-31; % kg
% Emax0=420; % ev
% qe=1.6e-19; % eV
% Emax=420.*qe; % J

20 % time of 1 = real time of 6.496120e-11 s, or 0.15915 of ...
% period
%
% velocity of 1 = a real velocity of 8.280787e+06 m/s
%
% distance of 1 = a real distance of 5.379299e-04 meters
25 %
% energy of 1 = a real energy of 420 eV
%
% efield of 1 = a real Efield of 0.78077 MV/m

30 % therefore, based on Valfells, et al. figure 5, we want the ...
% values (in the scale of the figure)
% to be as follows:
% Erf ~ 0 to 10
% Edc ~ 0 to 1.8
% which correspond to real values as follows (figure units to real...
% units
35 % conversion is 2.5:1):
% Erf ~ 0 to 25 MV/m
% Edc ~ 0 to 4.5 MV/m
% which can be translated to the normalized values of (normalized ...
% to real value conversion is 1.28e-6:1)
% Erf ~ 0 to 32
40 % Edc ~ 0 to 5.76

%...
-----

```

```

% Debugging
%...
-----...

45 clear all;
   clc;
   close all;
   seeIt=0;
   plotIt=0;
50 movieYes=1;
   %%
   %...
-----...

% Global Parameters - these are the only parameters that need to ...
   be
%   specified
55 %...
-----...

%
eMax0Arg=420; % eV
ksArg=1; % the smoothness parameter
dMax0Arg=3; % secondary emission
60 zetaInit=pi/2; % the impact angle
freq=2.45e+9; % Hz

voArg=1/sqrt(420/2); % initial velocity
phiArg=pi/2; % emission angle (pi/2 is normal to the surface)
65 psiMat=deg2rad([5 8 10 20 30 50 75]); % angle of obliqueness (...
   angle of Erf wrt surface - zero is parallel)

ErfMat=linspace(0,32,50)'; % the ranges of the E-fields. See ...
   notes above for
EdcMat=linspace(0,5.76,25)'; % explanation of units

70 %%
%...
-----...

% From the literature (Valfells, et al - Plasma Physics Jan 98)
%   this is the function way
%...
-----...

75 % phi is the injection angle for the emitted particle (pi/2 is ...
   normal to
%   the surface)Erf
% psi is the angle of the Erf with respect to surface (zero is ...
   parallel)
% theta is the phase angle of the Erf field

```

```

80 ax=@(Edc,Erf,psi,t,theta) -Edc-Erf.*sin(t+theta).*sin(psi);
   ay=@(Erf,theta,psi,t) -Erf.*sin(t+theta).*cos(psi);

   vx=@(Edc,Erf,phi,psi,t,theta,vo) vo.*sin(phi) - Edc.*t + Erf.*sin(...
       psi).*(cos(t+theta)-cos(theta));
   vy=@(Erf,phi,psi,t,theta,vo) vo.*cos(phi) + Erf*cos(psi).*(cos(t+...
       theta)-cos(theta));
85 x=@(Edc,Erf,phi,psi,t,theta,vo) -Edc.*t.^2/2 + t.*vo.*sin(phi)+Erf...
   .*cos(theta)...
   .*(-t + sin(t)).*sin(psi)-Erf.*sin(theta).*sin(psi)+Erf.*cos(t...
       ).*sin(theta).*sin(psi);

   y=@(Erf,phi,psi,t,theta,vo) t.*vo.*cos(phi) + Erf.*cos(psi).*(-t.*...
       cos(theta)-sin(theta)+sin(t+theta));
90 energy=@(Edc,Erf,phi,psi,t,theta,vo) 0.5.*(vx(Edc,Erf,phi,psi,t,...
   theta,vo).^2 ...
   +vy(Erf,phi,psi,t,theta,vo).^2);

   %%
95 %...
   -----...

   % Loop over different values of psi
   %...
   -----...

   ErfMat=ErfMat(2:end,1); % truncate off the first zero, since the...
       solvers
   EdcMat=EdcMat(2:end,1); % won't like zeros as the first ...
       arguments
100 if movieYes==1
    mov=avifile('oblique.avi','fps',5);
    end

105 for p=1:length(psiMat)
    psiArg=psiMat(p);

    %...
    -----...

    % The middle loop starts here - the goal is to set EDC to a value ...
    and dynamically
110 % vary ERF until we find a value of delta that is close enough ...
    to 1.
    % However, the two 'for' loop method will creep up on it - it ...
    will systematically
    % adjust Erf and Edc and plot the results with a plus or minus ...
    based on
    % growth or decay.

```

```

%...
-----

115     resultsCell=cell(length(ErfMat)*length(EdcMat),3);    % this ...
        stores the Edc vs Erf values & line markers
        amax=length(EdcMat);
        bmax=length(ErfMat);

120     % initialize the yield results matrices
        dPhAvgMat=0;
        dEnAvgMat=0;

        for a=1:amax
125         EdcArg=EdcMat(a,1);

            for b=1:bmax
130             ErfArg=ErfMat(b,1);

                % while abs(1-deltaAvg)>tol    % one way to do it is ...
                to dynamically adjust          %
                                                %   Erf to find the ...
                                                %   value that makes ...
                                                %   delta
135                                                %   within a specified ...
                                                tolerance

                %...
                -----

                % Now, let's solve the inner loop (sampling 50 times ...
                in the phase of the RF
                % field)
140             %...
                -----

                nmax=50;
                enList=zeros(nmax,1);    % initialize the storage ...
                vectors
                tcList=zeros(nmax,1);
145             dList=zeros(nmax,1);
                tcGuess=0.1;
                xtTheta=@(t,theta) x(EdcArg,ErfArg,phiArg,psiArg,t,...
                theta,voArg);

150             % a fast way to generate titles

```

```

conditions=strcat({'Erf = '},num2str(ErfArg),{'', Edc =...
    '},num2str(EdcArg), ...
    {'', \psi = '},num2str(rad2deg(psiArg)), '^{\circ}'...
    );

for n=0:nmax
155     thetaArg=2*pi*n/nmax;
        xt=@(t) xtTheta(t,thetaArg);
        % find the hoptime, associated impact energy and ...
        % impact angle
        tcList(n+1,1)=fzero(xt,tcGuess);
        tcGuess=tcList(n+1,1); % update the starting...
        % value for the fzero function
160     % while tcList(n+1,1) < 0.005
        %     tcGuess=tcGuess*2;
        %     tcList(n+1,1)=fzero(xt,tcGuess);
        % end

165     enList(n+1,1)=energy(EdcArg,ErfArg,phiArg,psiArg,...
        tcList(n+1,1),thetaArg,voArg);
        impactAngle=abs(vy(ErfArg,phiArg,psiArg,tcList(n...
        +1,1),thetaArg, voArg)/...
        vx(EdcArg,ErfArg,phiArg,psiArg,tcList(n+1,1),...
        thetaArg,voArg));
        zetaTilt=atan(impactAngle);

170     % find E1 and E2 for this case and the yield
        [e1,e2,deltaCase,eMaxCase]=sec_emission(eMax0Arg,...
        ksArg,dMax0Arg,zetaTilt,0);

        dList(n+1,1)=deltaCase(enList(n+1,1)*eMaxCase);

175     if seeIt==1
        disp(['iteration = ' num2str(n)])
        disp([' Hoptime = ' num2str(tcList(n+1,1))])
        disp([' hoptime/period is ' num2str(tcList(n+1,1)...
        *2*pi)])
        disp([' Energy = ' num2str(enList(n+1,1))])
180     disp([' Phase (degrees) = ' num2str(rad2deg(...
        thetaArg))])
        disp([' Yield = ' num2str(dList(n+1,1))])
        disp([' E1 = ' num2str(e1)])
        disp([' E2 = ' num2str(e2)])
        disp([' impact angle = ' num2str(rad2deg(zetaTilt))...
        ])
185     end
end

enAvg=mean(enList); % phase averaged energy
deltaAvg=mean(dList); % phase averaged yield
190 nrange=(0:1:nmax)';

```

```

if plotIt==1
scrsz = get(0,'ScreenSize'); % get the screen size
figure('Position',[scrsz(3)/4 scrsz(4)/4 scrsz(3)/2 ...
    scrsz(4)/2]); % make the figure in the middle of ...
    the screen
195 plot(nrange,enList);
    title(['Impact Energy vs Iteration (2*n*pi/nmax) for '...
        conditions]);
    xlabel('Iteration');
    ylabel('Energy');

200 figure('Position',[scrsz(3)/4 scrsz(4)/4 scrsz(3)/2 ...
    scrsz(4)/2]); % make the figure in the middle of ...
    the screen
    plot(nrange,dList);
    title(['Yield vs Iteration (2*n*pi/nmax) for ' ...
        conditions]);
    xlabel('Iteration');
    ylabel('Yield');
205 end

[e1,e2,deltaCase,eMaxCase]=sec_emission(eMax0Arg,ksArg...
    ,dMax0Arg,pi/2,0);

% store the two different yields in a matrix
210 dPhAvgMat=vertcat(dPhAvgMat,deltaAvg); % the phase ...
    averaged yield
dEnAvgMat=vertcat(dEnAvgMat,deltaCase(enAvg*eMax0Arg))...
    ; % the yield based on the phase-avg energy

% display the results
215 disp(['ERF = ' num2str(ErfArg)])
    disp(['EDC = ' num2str(EdcArg)])
    disp(['Psi = ' num2str(psiArg)])
    disp(['The phase averaged impact energy is ' num2str(...
        enAvg)])
    disp(['The phase averaged yield is ' num2str(deltaAvg)...
        ])
    disp(['The yield based on the phase-averaged energy is...
        ' num2str(deltaCase(enAvg*eMax0Arg))])

220 % find out if it's growth or decay and plot it with ...
    the appropriate
    % marker type

    if deltaAvg < 1
225 markerType='ob';
    elseif deltaAvg >= 1
        markerType='+r';
    end

230 % store the results in a cell array

```

```

        resultsCell{(a-1)*bmax+b,1}=EdcArg;
        resultsCell{(a-1)*bmax+b,2}=ErfArg;
        resultsCell{(a-1)*bmax+b,3}=markerType;

235     end
    end

240
    % plot the results at the very end

    scrsz = get(0,'ScreenSize'); % get the screen size
    figure('Position',[scrsz(3)/6 scrsz(4)/6 scrsz(3)/1.5 scrsz(4)...
        /1.5]); % figure in the middle of the screen
245 set(0,'defaulttextinterpreter','latex');
    % f = figure(1);
    axis('xy');
    %set(gca, 'Units', 'Inches', 'OuterPosition', [0.25 0.25 8 6])...
        ;
    %axis ('image');
250 %set(f, 'Units', 'Inches', 'PaperPosition', [0 0 8 6]);
    hold on;
    for d=1:size(resultsCell,1)
        plot(resultsCell{d,1}*((1e9/freq)*sqrt(400/eMax0Arg)...
            *(1/1.28)),resultsCell{d,2}*((1e9/freq)*sqrt(400/...
            eMax0Arg)*(1/1.28)),...
            resultsCell{d,3});
255     end

    xlabel({' ',' '};'$E_{dc, actual} [MV/m] \times (f/1 GHz)^{\...
        mbox{-} 1}(E_{max,0}/400 eV)^{\mbox{-} 1/2}$','FontSize'...
        ,12);
    ylabel({' '$E_{rf, actual} [MV/m]\times (f/1 GHz)^{\mbox{-}1}(E_{...
        {max,0}/400 eV)^{\mbox{-}1/2}$';' ',' '},'FontSize',12);
    title(['Susceptibility Curve for $\psi = $' num2str(rad2deg(...
        psiArg)) '$^{\circ}$ \& $\delta_{max,0} = $' num2str(dMax0Arg)...
        ],...
260     'FontSize',14);
    [hx,hy]=format_ticks(gca,'$$','$$');
    hold off;
    savefigs(['oblique_PSI=' num2str(rad2deg(psiArg)) 'deg']);
    if movieYes==1
265         winsize=get(gcf,'Position');
            winsize(1:2)=[0 0];
            F(p)=getframe(gcf,winsize);
            mov=addframe(mov,F(p));
    end
270 close all;

    figure('Position',[scrsz(3)/4 scrsz(4)/4 scrsz(3)/2 scrsz(4)...
        /2]); % figure in the middle of the screen

```

```

hold on;
plot(dPhAvgMat,'b','LineWidth',2);
275 plot(dEnAvgMat,'r','LineWidth',2);
title(['Yield for  $\psi =$  ' num2str(rad2deg(psiArg)) '^...\
      circ$ \&  $\Delta_{\{max,0\}} =$  ' num2str(dMax0Arg)'],...
      'FontSize',14);
xlabel({' ' ' '; 'Edc/Erf pair'},'FontSize',14);
ylabel({'Yield'; ' ' ' '},'FontSize',14);
280 [hx,hy]=format_ticks(gca,'$$','$$');
legend('$\theta$ averaged  $\Delta$ ','$\Delta$ based on  $\dots$ 
      theta$ avg energy');
savefigs(['yield_PSI=' num2str(rad2deg(psiArg)) 'deg']);
close all;
end
285 if movieYes==1
mov=close(mov);
end

```

## Appendix D. Input File for the Oblique Case in ICEPIC

Listing D.1. Sample Input File With  $\psi = 5^\circ$

```
[Defaults]
2 ENERGY=1.5e6
  EDC=0.125e6
  sinpsi=0.0872 ; sin(psi) is a constant for each simulation
  ; this is based on fichtl's original input files and is meant to ...
    expand it to apply to oblique
  ; fields (8 Dec 08)
7
[Variables]
  c0=299792458.0
  pi=3.141592653589793
  eps0=8.85418781762E-12
12 me=9.1093897E-31
  qe=1.60217738E-19
  test=1
  fc=2.45E9
  lamda0=c0/fc
17 ez=EDC
  energy=ENERGY
  dz=lamda0/3000
  PMLdepth=int((.025*lamda0)/dz+.5)
  Nx=50
22 Nz=300
  xmin=0
  xmax=Nx*dz
  zmin=0
  zmax=Nz*dz
27 dt=0.99*dz/(c0*sqrt(2))
  period=int(1/fc/dt)
  maxstep=15*period
  dumpint=period/30
  numstart=0*period
32 numstop=3*period
  hoptime=(2*me/qe/ez)*sqrt(2*qe*420/me)*0.8509035245
  hopdist=sqrt(2*qe*420/me)*hoptime
  Ndielect=10*dz
  print "Hop time=", hoptime
37 print "Hop distance=", hopdist
  print "TimeSteps/Hoptime=", hoptime/dt
  print "Hop distance/dz=", hopdist/dz

[Cartesian]
42 ig_dir=(0,1,0)
  default_e=(0.,0.,-ez)
  ;flattop=.5/fc
  ;amp2=0
  tstart=0.0
47 tstop=10*period
```

```

c0=1
c1=(ENERGY/-EDC)*sinpsi
frequency=fc
ramp=5*dt
52 [XGrid1]
range=Uniform(xmin-3*dz,xmax+3*dz,Nx+6)

[YGrid1]
57 range=Uniform(0,1,1)

[ZGrid1]
range=Uniform(zmin,zmax,Nz)

62 [Symmetry]
;symmetry=(xmin,-1.,zmin-10*dz,xmax,2.,zmax+10*dz)
periodic1=(X,xmin,xmax)
;sym mode=(1.0,0.0,0.0)

67 [Time]
dt=dt
step_max=maxstep
courant_value=.95
72 kill_if_below_parts=5
kill_if_above_parts=2e6

[ShapeN]
77 shape=Box(xmin,xmin,zmin,xmax,xmax,zmax)

[ShapeN]
;Dielectric on RHS of system
shape=Box(xmin,0.0,zmax-4*dz-PMLdepth*dz-Ndielect,xmax,1.0,zmax-4*...
dz-PMLdepth*dz)
material=dielectric

82 [ShapeN]
;Dielectric on LHS of system
shape=Box(xmin,0.0,zmin+4*dz+PMLdepth*dz,xmax,1.0,zmin+PMLdepth*dz...
+Ndielect+4*dz)
material=dielectric

87 [MaterialN]
name=dielectric
epsilon=1.001

92 [ParticlesN]
;Secondary emitter on dielectric on RHS of system
shape=Box(xmin-dz,0.0,zmax-4.25*dz-PMLdepth*dz-Ndielect,xmax,1.0,...
zmax-3.75*dz-PMLdepth*dz-Ndielect)
method=SECONDARY
sec_coefficient=3

```

```

97 sec_energy=2.1/test
    sec_threshold=1/test
    sec_refl=0.03
    sec_scatter=0.07
    sec_energy_max_yield=420/test
102 sec_ks=1
    q=-qe/test
    mass=me/test
    dir=2

107 [ParticlesN]
    ;Particle emitter on dielectric on RHS of system
    shape=Box(xmin-dz,0.0,zmax-4.25*dz-PMLdepth*dz-Ndielect,xmax,1.0,...
        zmax-3.75*dz-PMLdepth*dz-Ndielect)
    method=BEAM
    temp=2.1/test
112 energy=0.0/test
    random=1
    q=-qe/test
    mass=me/test
    current=1000/test
117 inject_interval=100
    flattop=.5/fc
    amp2=0
    tstop=.5/fc
    smooth=1
122 dir=2

    [PlanewaveN]
    ;Generates Planewave from xmin to xmax across system
    shape=Box(xmin-2*dz,0.0,zmin+PMLdepth*dz+2*dz,xmax+2*dz,1.0,zmax-...
        PMLdepth*dz-2*dz)
127 theta=180.0
    phi=0.0
    psi=180.0
    frequency=fc
    origin=(xmin,0.0,zmin+2*dz+dz*PMLdepth)
132 E0=energy

    [Expert]
    ;cell_mult=12 ;not sure what this parameter is...
    requested_max_num_particles=3e6
137 self_fields=0

    [BoundN]
    ;PML on LHS of system
    method=PML
142 depth=PMLdepth
    R=1.0E-4
    taper=0
    order=2
    dir=2

```

```

147 shape=Box(xmin,0,zmin-dz/2,xmax,1.0,zmin+dz/2)

    [BoundN]
    ;PML on RHS of system
    method=PML
152 depth=PMLdepth
    R=1.0E-4
    taper=0
    order=2
    dir=2
157 shape=Box(xmin,0,zmax-dz/2,xmax,1.0,zmax+dz/2)

    [DumpN]
    dump_format=FIELD
162 dump_plane=1
    dump_value=0
    fieldflags=1-1-1-2-p-1
    dump_interval=dumpint
    shape=Box(xmin,xmin,(zmax-PMLdepth*dz-Ndielect-5*dz)-(zmin+...
        PMLdepth*dz+Ndielect+5*dz)/2,xmax,xmax,zmax-PMLdepth*dz-...
        Ndielect-1*dz)
167 dump_in_PML=0
    ;dump_exclude_static=0 ;not supported by current version
    nstart=numstart
    nstop=numstop
    ;
172 ;[DumpN]
    ;dump_format=CQUADS
    ;shape=Box(xmin,xmin,zmin,xmax,xmax,zmax)
    ;nstop=0
    ;
177 ;[DumpN]
    ;dump_format=POWER
    ;dump_plane=2
    ;dump_value=zmax-PMLdepth*dz-3*dz
    ;dump_name=powerT
182 ;shape=Box(xmin,xmin,zmin,xmax,xmax,zmax)
    ;nstart=22*period
    ;nstop=25*period
    ;
    ;[DumpN]
187 ;dump_format=POWER
    ;dump_plane=2
    ;dump_value=zmin+3*dz+PMLdepth*dz
    ;dump_name=powerB
    ;shape=Box(xmin,xmin,zmin,xmax,xmax,zmax)
192 ;nstart=22*period
    ;nstop=25*period
    ;
    ;[DumpN]
    ;dump_format=POWER

```

```

197 ;dump_plane=2
    ;dump_value=zmin+1*dz+PMLdepth*dz
    ;dump_name=powerR
    ;shape=Box(xmin,xmin,zmin,xmax,xmax,zmax)
    ;nstart=22*period
202 ;nstop=25*period
    ;
    ;[DumpN]
    ;dump_format=PROBE
    ;dump_interval=1
207 ;p=((xmax-xmin)/2,0,zmax-5.25*dz-PMLdepth*dz-Ndielect)
    ;
    ;[DumpN]
    ;dump_format=PROBE
    ;dump_interval=1
212 ;p=((xmax-xmin)/2,0,zmax-4.25*dz-PMLdepth*dz-Ndielect)
    ;
    ;[DumpN]
    ;dump_format=J_DOT_E
    ;avg_interval=1000
217 ;dump_interval=100
    ;nstart=22*period
    ;nstop=25*period
    ;shape=Box(xmin,xmin,(zmax-PMLdepth*dz-Ndielect-5*dz)-(zmin+...
        PMLdepth*dz+Ndielect;+5*dz)/2,xmax,xmax,zmax-PMLdepth*dz-...
        Ndielect-5*dz)

222 ;[DumpN]
    ;dump_format=DENSITY
    ;species_num=0
    ;dump_interval=20
    ;nstart=14*period
227 ;nstop=15*period
    ;dump_local=0
    ;shape=Box(xmin,xmin,(zmax-PMLdepth*dz-Ndielect-5*dz)-(zmin+...
        PMLdepth*dz+Ndielect+5*dz)/2,xmax,xmax,zmax-PMLdepth*dz-...
        Ndielect-5*dz)

```

**Appendix E. Mathematica<sup>®</sup> Notebook for the Approximation  
of the Theoretical Power Deposited on the Surface of a  
Dielectric**

CODE BEGINS ON NEXT PAGE

# Verboncoeur Inputs for ICEPIC results

- This notebook accumulates the results presented by Verboncoeur in IEEE transactions on Plasma Science, Vol. 28, No. 3, June 2000 pp 529-536. We want to develop a working form for interpreting the results of the ICEPIC runs.

We assume that our inputs will include:

Basic:

**N** = number of pseudo particles

**L** = electrode separation

**$\Delta t$**  = integration time step

**$\beta$**  = particle weighting

Case specific inputs

**$E_{Rf}$**  = Rf field amplitude

**f** = frequency of Rf field

**T** = temperature of emitted electrons  
or alternatively

**$v_t$**  = thermal velocity

The final input is the ejection current density,  **$J_0$**

$$J_0 = \sqrt{\pi} n_0 e v_t / 2$$

Since we have assigned  $v_t$ , the sole parameter is  $n_0$ . Our purpose is to lay out the methodology to make this assignment and estimate the power deposited on the surface of a dielectric in the space charge case. Therefore, we must first start by finding the value of  $n_0$  by integrating Verboncoeur's equation (15).

```
In[45]:= Clear["Global`*"]
```

```

In[46]:= dx = 3.05910671429 * 10 ^ (-5); (*the length in the x direction*)
dy = 1*^-2;
zmax = 0.0016; (*the total length in z for the interaction
                space of our system*)

vt = 9.92*^5;
qe = 1.602*^-19;
eps = 8.8542*^-12;
me = 9.11*^-31;


$$\omega_p[n\_ ] = \sqrt{n * qe ^ 2 / (eps * me) } ;$$

nmacro = 1*^5; (*from the ICEPIC run - ice.stat file *)
ratio = 1.2384*^3; (*this is the ratio of macroparticles to
                    electrons - fixed for a given inject
                    current *)
ntot = nmacro * ratio; (*this gives us the total number of real
                        electrons in the system*)
nzideal = ntot / (dx * dy); (* this is the ideal total number of
                              real electrons in particles/m^3 -
                              we need to set the integral of
                              Verboncoeur's equation 15 equal
                              to this *)

Print["Ideal Nz = ", nzideal]

Ideal Nz = 4.04824 × 1014

In[57]:= int2 = Integrate[1 / (1 + a * z) ^ 2, {z, 0, zmax}];
a1 =  $\sqrt{n * qe ^ 2 / (eps * me * vt ^ 2) } ;$ 
f[n_] := Evaluate[(int2 * n /. a → a1)];
f[nn];

In[61]:= f[5.29 * 10 ^ 20] (*this is the number that should match up with
                            nzideal*)

Out[61]= 4.043 × 1014

```

- We consider the y-component of the velocity and assume the injected value of this component,  $v_{0y}$ , is zero.

```
f = 2.45 10^9; Efrf = 3.0 × 10^6; n = 5.29 * 10^20; shield = 1;
(* Shield == 1, shielding case for G, Shield == 0 ,
   no shielding *)
```

```
(* the n value here is n0 from the above calculations*)
ω = 2 π f;
qe = 1.6 × 10^(-19);
me = 9.1 × 10^(-31);
eps = 8.8542 × 10^(-12);
toev = 1. / (1.6 × 10^(-19));
dx = 3.05910671429 * 10^(-5);
dy = 1;
c0 = 2.99792 * 10^8;
```

```
vrf = qe * Efrf / (ω me); kT = 2.8 / toev; vt = √(2 kT / me);
Print["The Rf electric field velocity is vrf = "
      , vrf, " [m/sec]"];
Print["The thermal velocity is vt = ", vt, " [m/sec]"];
```

```
(* Plasma frequency *)
wp[n_] := √(n qe^2 / (eps me))
```

```
(* Efx E field due to surface charge *)
Efx[n_] := √(2 kT n / eps);
Print["x E-field ", Efx[n]]
Print["x E-field velocity ", qe Efx[n] / (me ω)]
```

```
(* cycle time or bounce time Eqn[19] *)
τ[v_, n_] := √(2 π) Exp[v^2 / (2 vt^2)] Erf[√(v^2 / (2 vt^2))] /
            wp[n];
```

```
(* Shielding function *)
Gshield[U_, shield_] := shield * (1 - 2 √2 / √π NIntegrate
    [Cos[√(2 π) U Exp[y^2] Erf[y]] Exp[-2 y^2],
```

```

      {y, 0, Infinity}]] + (1 - shield) * (1. - Exp[-U^2]);

(* Current density *)
jZero[n_] := Sqrt[pi] n qe vt / 2.;
Print["Current Density jZero = ", jZero[n], " A/m^2"]

Print["Ratio of Plasma Frequency to Rf frequency ", wp[n] / w];
(* Average Impact energy *)
ai[U_] := me * vrf^2 / 2 * Gshield[U, shield];
Print["Average Impact energy in ", ai[w/wp[n]] * toev, " eV "]
Print["Maximum impact energy = ", 2 me * vrf^2 toev, " eV"];
(* Average Power deposited *)

powerDeposited[n_] := ai[w/wp[n]] * jZero[n] / qe;
Print["Power deposited ", powerDeposited[n], " W/m^2"]
Print["Average Power Deposited ", powerDeposited[n] *
  dx * dy, " W"]

uenergy = 0.5 * eps * Efrf^2;
poynting = c0 * uenergy;
pththeory = dx * dy * poynting;
Print["Percentage of power deposited ", powerDeposited[n] * dx

The Rf electric field velocity is vrf =  $3.42652 \times 10^7$  [m/sec]
The thermal velocity is vt = 992278. [m/sec]
x E-field  $7.31656 \times 10^6$ 
x E-field velocity  $8.3568 \times 10^7$ 
Current Density jZero =  $7.4431 \times 10^7$  A/m2
Ratio of Plasma Frequency to Rf frequency 84.2183
Average Impact energy in 3.08009 eV
Maximum impact energy = 13355.5 eV
Power deposited  $2.29254 \times 10^8$  W/m2
Average Power Deposited 7013.14 W
Percentage of power deposited 1.91927%

```

## Bibliography

- [1] Ang, L.K., Y.Y. Lau, R.A. Kishek, and R.M. Gilgenbach. “Power deposited on a dielectric by multipactor”. *IEEE Transactions on Plasma Science*, 26(3):pp. 290–295, Jun 1998. ISSN 0093-3813.
- [2] Bailey, William F. and William Wood. “High Powered Microwave Systems, Propagation”. A short course presented to the Directed Energy community.
- [3] Barker, Robert J. and Edl Schamiloglu. *High-Power Microwave Sources and Technologies*. IEEE Press, New York, 2001. ISBN 0-7803-6006-0.
- [4] Bettencourt, Dr. Matthew T., Jr. Lt. Joseph D. Blahovec, and Mr. Lester Bowers. *ICEPIC v. Jul08b User’s Manual*. Directed Energy Directorate, High-Powered Microwave Division, Center for Plasma Theory and Computation, July 2008.
- [5] Birdsall, C.K. and A.B. Langdon. *Plasma Physics Via Computer Simulation*. Adam Hilger, Bristol, 1991. ISBN 0-07-005371-5.
- [6] Castañeda, S. I., N. Díaz, D. Raboso, I. Montero, L. Galán, and F. Rueda. “Effects of air exposure on ion beam assisted TiN:O coatings to prevent multipactor”. *Journal of Vacuum Science & Technology A: Vacuum, Surfaces, and Films*, 21(6):2007–2012, 2003. URL <http://link.aip.org/link/?JVA/21/2007/1>.
- [7] Fichtl, Christopher. *Self-Consistent Simulation of Multipactor Discharges at HPM Dielectric Windows*. Technical report, Air Force Research Lab, February 2007.
- [8] Kennedy, K., B. Harteneck, G. Millos, M. Benapfl, F. King, and R. Kirby. “TiN coating of the PEP-II low-energy aluminum arc vacuum chambers”. *Particle Accelerator Conference, 1997. Proceedings of the 1997*, 3:3568–3570 vol.3, May 1997.
- [9] Kim, H. C. and J. P. Verboncoeur. “Time-dependent physics of a single-surface multipactor discharge.” *Physics of Plasmas*, 12(12), 2005. ISSN 1070664X. URL <http://search.ebscohost.com/login.aspx?direct=true&db=aph&AN=19406254&site=ehost-live>.
- [10] Kishek, R. and Y. Y. Lau. “Interaction of Multipactor Discharge and rf Circuit”. *Phys. Rev. Lett.*, 75(6):pp. 1218–1221, Aug 1995.
- [11] Kishek, R. A. and Y. Y. Lau. “Multipactor Discharge on a Dielectric”. *Phys. Rev. Lett.*, 80(1):193–196, Jan 1998.

- [12] Kishkek, R.A. and Y.Y. Lau. “Multipactor discharge on metals and dielectrics: Historical review and recent theories.” *Physics of Plasmas*, 5(5):pp. 2120–2126, May 1998. ISSN 1070664X. URL <http://search.ebscohost.com/login.aspx?direct=true&db=aph&AN=4260470>\newline\&site=ehost-live.
- [13] Montero, I., S. H. Mohamed, M. Garcia, L. Galan, and D. Raboso. “Effect of surface reactions of low-energy carbon ions on the secondary electron emission of TiN:O thin films”. *Journal of Applied Physics*, 101(11):113306, 2007. URL <http://link.aip.org/link/?JAP/101/113306/1>.
- [14] Sazontov, A., V. Semenov, M. Buyanova, N. Vdovicheva, D. Anderson, M. Lisak, J. Puech, and L. Lapierre. “Multipactor discharge on a dielectric surface: Statistical theory and simulation results.” *Physics of Plasmas*, 12(9), 2005. ISSN 1070664X. URL <http://search.ebscohost.com/login.aspx?direct=true&db=aph&AN=18636457>\newline\&site=ehost-live.
- [15] Valfells, A., L. K. Ang, Y. Y. Lau, and R. M. Gilgenbach. “Effects of an external magnetic field, and of oblique radio-frequency electric fields on multipactor discharge on a dielectric.” *Physics of Plasmas*, 7(2):pp. 750–757, Feb 2000. ISSN 1070664X. URL <http://search.ebscohost.com/login.aspx?direct=true&db=aph&AN=4416473>\newline\&site=ehost-live.
- [16] Valfells, A., J.P. Verboncoeur, and Y.Y. Lau. “Space-charge effects on multipactor on a dielectric”. *Plasma Science, IEEE Transactions on*, 28(3):pp 529–536, Jun 2000. ISSN 0093-3813.
- [17] Vaughan, J.R.M. “A new formula for secondary emission yield”. *Electron Devices, IEEE Transactions on*, 36(9):pp. 1963–1967, Sep 1989. ISSN 0018-9383.
- [18] Vaughan, R.M. “Secondary emission formulas”. *Electron Devices, IEEE Transactions on*, 40(4):830–, Apr 1993. ISSN 0018-9383.
- [19] Verboncoeur, John P. “The Plasma Theory and Simulation Group”. URL <http://ptsg.eecs.berkeley.edu/>.

## Vita

Capt Neil Rogers was born in Tulsa, Oklahoma. After graduating with honors from Union High School, he studied Electrical Engineering at the University of Tulsa. He graduated Cum Laude with his Bachelor's Degree in Electrical Engineering in May of 2003. Capt Rogers commissioned into the United States Air Force in August of 2004 through Officer Training School (OTS) at Maxwell AFB, Montgomery, Alabama. Following OTS, he was assigned to the National Air and Space Intelligence Center (NASIC) where he worked in remote sensing. Following his assignment to NASIC, he entered graduate school at the Air Force Institute of Technology (AFIT) in August of 2007 and he is currently completing his Master's Degree. His anticipated follow-on assignment is to the High Powered Microwave Division of the Air Force Research Labs (AFRL/RDHE) at Kirtland AFB, New Mexico.

# REPORT DOCUMENTATION PAGE

*Form Approved*  
*OMB No. 0704-0188*

The public reporting burden for this collection of information is estimated to average 1 hour per response, including the time for reviewing instructions, searching existing data sources, gathering and maintaining the data needed, and completing and reviewing the collection of information. Send comments regarding this burden estimate or any other aspect of this collection of information, including suggestions for reducing this burden to Department of Defense, Washington Headquarters Services, Directorate for Information Operations and Reports (0704-0188), 1215 Jefferson Davis Highway, Suite 1204, Arlington, VA 22202-4302. Respondents should be aware that notwithstanding any other provision of law, no person shall be subject to any penalty for failing to comply with a collection of information if it does not display a currently valid OMB control number. **PLEASE DO NOT RETURN YOUR FORM TO THE ABOVE ADDRESS.**

<b>1. REPORT DATE</b> ( <i>DD-MM-YYYY</i> ) 27-03-2009		<b>2. REPORT TYPE</b> Master's Thesis		<b>3. DATES COVERED</b> ( <i>From — To</i> ) Aug 2007 — Mar 2009		
<b>4. TITLE AND SUBTITLE</b>  Electron Multipactor: Theory Review, Comparison and Modeling of Mitigation Techniques in ICEPIC				<b>5a. CONTRACT NUMBER</b>		
				<b>5b. GRANT NUMBER</b>		
				<b>5c. PROGRAM ELEMENT NUMBER</b>		
<b>6. AUTHOR(S)</b>  Neil G. Rogers, Capt, USAF				<b>5d. PROJECT NUMBER</b> 08ENP306		
				<b>5e. TASK NUMBER</b>		
				<b>5f. WORK UNIT NUMBER</b>		
<b>7. PERFORMING ORGANIZATION NAME(S) AND ADDRESS(ES)</b> Air Force Institute of Technology Graduate School of Engineering and Management (AFIT/EN) 2950 Hobson Way WPAFB OH 45433-7765				<b>8. PERFORMING ORGANIZATION REPORT NUMBER</b>  AFIT/GE/ENP/09-M02		
<b>9. SPONSORING / MONITORING AGENCY NAME(S) AND ADDRESS(ES)</b> AFRL/RDHE (Dr. Keith Cartwright) 3550 Aberdeen Ave SE Kirtland AFB, NM 87117-5776 246-9101, keith.cartwright@kirtland.af.mil				<b>10. SPONSOR/MONITOR'S ACRONYM(S)</b> AFRL/RDHE		
<b>11. SPONSOR/MONITOR'S REPORT NUMBER(S)</b>				<b>11. SPONSOR/MONITOR'S REPORT NUMBER(S)</b>		
<b>12. DISTRIBUTION / AVAILABILITY STATEMENT</b>  APPROVED FOR PUBLIC RELEASE; DISTRIBUTION UNLIMITED.						
<b>13. SUPPLEMENTARY NOTES</b>						
<b>14. ABSTRACT</b>  Mitigation approaches for single surface multipactor at dielectric windows are investigated using Particle-In-Cell (PIC) simulations. Initially baseline susceptibility diagrams are constructed analytically and compared with self-consistent, dynamic system trajectories. The power deposited on the surface of a dielectric window in an HPM system is considered using three different methods and the results of PIC simulations. Geometric mitigation is then considered by varying the window orientation with respect to the HPM electric field. Small angular deviations, less than 20 degrees, from the nominal case of normal incidence show dramatic changes in the susceptibility diagram. A materials approach to mitigation is then considered. Titanium Nitride, TiN, coatings applied to the dielectric surface can substantially reduce the secondary emission yield. Representative modifications of the secondary emission yield are simulated and the resulting susceptibility diagrams are discussed.						
<b>15. SUBJECT TERMS</b>  Electron Multipactor, Multipactor, Multipactor Mitigation, Dielectric Surface, HPM Systems, High-Powered Microwave Systems, Thing Film Coatings, Oblique Incidence						
<b>16. SECURITY CLASSIFICATION OF:</b>			<b>17. LIMITATION OF ABSTRACT</b>	<b>18. NUMBER OF PAGES</b>	<b>19a. NAME OF RESPONSIBLE PERSON</b>	
a. REPORT	b. ABSTRACT	c. THIS PAGE			Dr. William F. Bailey	
U	U	U	U	117	<b>19b. TELEPHONE NUMBER</b> ( <i>include area code</i> ) (937) 255-3636, x4501; william.bailey@afit.edu	